

AD-A033 857

DENVER RESEARCH INST COLO  
THERMOMECHANICAL PROCESSING OF NICKEL BASE ALLOY AF2-1DA USING --ETC(U)  
JUN 76 R H WITTMAN

F/G 11/6  
N62269-74-C-0281

UNCLASSIFIED

DRI-5110

NADC-76321-30

NL

| OF |  
AD  
A033857



END

DATE  
FILMED

2-77

ADA033857



# REPORT

DRI No. 5110 ✓

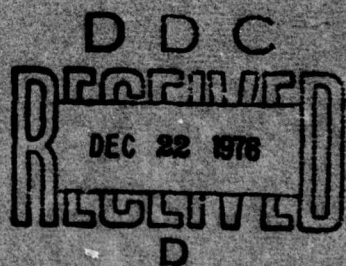
Final Technical Report

Contract No. N62269-74-C-0281

Naval Air Development Center

June 1976

## THERMOMECHANICAL PROCESSING OF NICKEL BASE ALLOY AF2-1DA USING SHOCK WAVE DEFORMATION



UNIVERSITY OF DENVER • DENVER RESEARCH INSTITUTE

**DISTRIBUTION STATEMENT A**

Approved for public release;  
Distribution Unlimited

DRI No. 5110

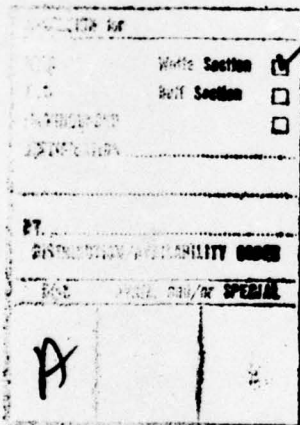
THERMOMECHANICAL PROCESSING OF NICKEL BASE ALLOY AF2-1DA USING SHOCK  
WAVE DEFORMATION

Final Technical Report

Prepared under contract N62269-74-C-0281  
Naval Air Development Center  
Warminster, Pennsylvania 18974

for

Naval Air Systems Command  
Department of the Navy  
Washington, D. C. 20361



- Submitted by -

University of Denver  
Denver Research Institute  
Denver, CO 80210

June 30, 1976

D D C  
RECORDED  
DEC 22 1976  
RECORDED  
D

Approved for the Director by:

Charles E. Lundin  
Charles E. Lundin, Ph.D.  
Head, Metallurgy and Materials Science  
Division

Prepared by:

Robert H. Wittman  
Robert H. Wittman  
Research Metallurgist

APPROVED FOR PUBLIC RELEASE: DISTRIBUTION UNLIMITED.

## SECURITY CLASSIFICATION OF THIS PAGE (When Data Entered)

19) REPORT DOCUMENTATION PAGE			READ INSTRUCTIONS BEFORE COMPLETING FORM
1. REPORT NUMBER NADC 76321-30	2. GOVT ACCESSION NO.	3. RECIPIENT'S CATALOG NUMBER	
4. TITLE (and Subtitle) THERMOMECHANICAL PROCESSING OF NICKEL BASE ALLOY AF2-1DA USING SHOCK WAVE DEFORMATION		5. DATE OF REPORT & PERIOD COVERED Final Technical Report 20 Mar 74 - 30 Jun 75	
6. AUTHOR(s) Robert H. Wittman		7. CONTRACT OR GRANT NUMBER(s) N62269-74-C-0281 New	
8. PERFORMING ORGANIZATION NAME AND ADDRESS Denver Research Institute University of Denver Denver, CO 80210		10. PROGRAM ELEMENT, PROJECT, TASK AREA & WORK UNIT NUMBERS 62269/TM4/0741/74	
11. CONTROLLING OFFICE NAME AND ADDRESS Naval Air Development Center Department of the Navy Warminster, PA 18974		12. REPORT DATE 30 June 1976	
14. MONITORING AGENCY NAME & ADDRESS (if different from Controlling Office) Naval Air Development Center Department of the Navy Warminster, PA 18974		13. NUMBER OF PAGES 50 1258P	
15. SECURITY CLASS. (of this report) Unclassified			
15a. DECLASSIFICATION/DOWNGRADING SCHEDULE			
16. DISTRIBUTION STATEMENT (of this Report) Approved for Public Release; Distribution Unlimited 14 DRI-5110			
17. DISTRIBUTION STATEMENT (of the abstract entered in Block 20, if different from Report)			
18. SUPPLEMENTARY NOTES			
19. KEY WORDS (Continue on reverse side if necessary and identify by block number) Nickel Base Alloy Shock Hardening Thermomechanical Processing			
20. ABSTRACT (Continue on reverse side if necessary and identify by block number) An investigation was conducted to study the effects of shock wave deformation and heat treatment on the mechanical properties of nickel base superalloy AF2-1DA. Shock wave deformation having a transient volume strain of 23.6% was generated by an explosively induced 500 Kbar shock wave. The shock wave deformation was introduced to AF2-1DA plates in the solution treated condition and after various solution treatments and gamma prime heat treatments. Carbide and/or final aging heat treatments were conducted			

108600 ✓ An

SECURITY CLASSIFICATION OF THIS PAGE(When Data Entered)

after shock wave deformation processing. For comparison and evaluation of results AF2-1DA plates from the same lot of material were thermally processed using the standard solution treatment and aging sequences. Tensile, stress-rupture, and low cycle fatigue testing was conducted on shock wave processed and thermally processed samples. In general the result was to increase the yield strength by up to 15% and the tensile strength by 3-5% at the 1400°F test temperature for the shock wave processed alloy relative to the thermally processed alloy. This strength increase was accomplished with a 7% increase in elongation and 20% increase in the reduction of area. Such increases indicate a substantial increase in toughness of the shock wave processed alloy. The increase in toughness of the shock wave processed material was manifested by measured improvements in the stress-rupture life and the low cycle fatigue life. These property enhancements are achieved using a transient deformation that results in very little permanent distortion of the workpiece. The implication to commercial processing was demonstrated by shocking a steel disk simulating a cast, forged, or powder compacted turbine wheel preform.

SECURITY CLASSIFICATION OF THIS PAGE(When Data Entered)

ABSTRACT

An investigation was conducted to study the effects of shock wave deformation and heat treatment on the mechanical properties of nickel base superalloy AF2-1DA. Shock wave deformation having a transient volume strain of 23.6% was generated by an explosively induced 500 Kbar shock wave. The shock wave deformation was introduced to AF2-1DA plates in the solution treated condition and after various solution treatments and gamma prime heat treatments. Carbide and/or final aging heat treatments were conducted after shock wave deformation processing. For comparison and evaluation of results AF2-1DA plates from the same lot of material were thermally processed using the standard solution treatment and aging sequences. Tensile, stress-rupture, and low cycle fatigue testing was conducted on shock wave processed and thermally processed samples. In general the result was to increase the yield strength by up to 15% and the tensile strength by 3-5% at the 1400°F test temperature for the shock wave processed alloy relative to the thermally processed alloy. This strength increase was accomplished with a 7% increase in elongation and 20% increase in the reduction of area. Such increases indicate a substantial increase in toughness of the shock wave processed alloy. The increase in toughness of the shock wave processed material was manifested by measured improvements in the stress-rupture life and the low cycle fatigue life. These property enhancements are achieved using a transient deformation that results in very little permanent distortion of the workpiece. The implication to commercial processing was demonstrated by shocking a steel disk simulating a cast, forged, or powder compacted turbine wheel preform.

TABLE OF CONTENTS

	<u>Page</u>
ABSTRACT . . . . .	i
LIST OF TABLES . . . . .	iii
LIST OF FIGURES . . . . .	iv
I. <u>INTRODUCTION</u> . . . . .	1
II. <u>SHOCK WAVE DEFORMATION</u> . . . . .	2
2.1 SHOCK WAVES IN METALS . . . . .	2
2.2 SHOCK WAVE EFFECTS . . . . .	4
III. <u>EXPERIMENTAL DETAILS</u> . . . . .	9
3.1 MATERIAL . . . . .	9
3.2 PHYSICAL METALLURGY OF AF2-1DA . . . . .	10
3.3 SHOCK WAVE DEFORMATION OF AF2-1DA . . . . .	11
3.4 SHOCK WAVE TREATMENT PROCEDURE . . . . .	18
3.5 MECHANICAL TESTING PROCEDURE . . . . .	21
IV. <u>RESULTS AND DISCUSSION</u> . . . . .	24
4.1 TENSILE PROPERTIES OF AF2-1DA . . . . .	24
4.2 TENSILE PROPERTIES OF AF2-1DA AFTER SHOCK WAVE TMP . . . . .	27
4.3 STRESS RUPTURE BEHAVIOR . . . . .	33
4.4 LOW CYCLE FATIGUE BEHAVIOR . . . . .	38
4.5 SHOCK WAVE PROCESSING OF A DISK CONFIGURATION . . . . .	38
V. <u>SUMMARY AND CONCLUSIONS</u> . . . . .	46

## References

## Distribution List

LIST OF TABLES

<u>Table No.</u>		<u>Page</u>
I	Chemical Composition of AF2-1DA Alloy . . . . .	9
II	Symbols Used in Hugoniot and Shock Relationships. . . . .	13
III	Calculated Hugoniot Parameters for AF2-1DA. . . . .	16
IV	Pressure, Volume and Equivalent Strain Parameters for AF2-1DA Alloy . . . . .	18
V	Room and Elevated Temperature Tensile Properties of AF2-1DA in the STA Condition. . . . .	25
VI	Room and Elevated Temperature Tensile Properties of AF2-1DA after Shock-Wave TMP. . . . .	29
VII	Tensile Properties of AF2-1DA - Effect of $\gamma'$ Before Shock Treatment and Effects of Carbide Aging After Heat Treatment	31
VIII	Stress Rupture Behavior for Thermally Processed and Shock Wave Thermomechanically Processed AF2-1DA . . . . .	35
IX	Influence of Shock Wave TMP on the Low Cycle Fatigue Life of AF2-1DA. . . . .	39

LIST OF FIGURES

<u>Figure No.</u>		<u>Page</u>
1	Pressure-Time Profile for One Dimensional Shock . . . . .	3
2	Relative Displacement of Atom in a Cubic Lattice Due to Planar Shock Wave . . . . .	5
3	Configuration of AF2-1DA Sample and Tooling for Shock Wave TMP	14
4	Configuration of Explosive-Flyer Plate Assembly, Specimen Assembly and Recovery Pit for Shock Wave TMP of AF2-1DA . . .	20
5	AF2-1DA Tensile and Stress Rupture Specimen Design . . . . .	22
6	AF2-1DA Low-Cycle Tension-Fatigue Specimen Design . . . . .	23
7	Typical AF2-1DA Alloy Microstructures after STA Processing (Carbide Stringer of the magnitude shown in Figures 7 and 10 were not observed at the beginning of the program) . . . . .	26
8	Tensile Properties of AF2-1DA Alloy after Various Treatments. . . . .	28
9	STA Processed AF2-1DA Alloy Microstructure from Stress-Rupture Sample Revealing Grain Boundary Ruptures Originating at Carbide Stringer (500X) . . . . .	36
10	ST + $\gamma'$ + S + C + F Processed AF2-1DA Alloy Microstructures from Stress Rupture Sample Revealing Grain Boundary Ruptures Originating at Carbide Stringers and the Specimen Surfaces (100X) . . . . .	36
11	Creep Test Results at 1400°F and 85,000 psi for AF2-1DA Alloy after Various Processing Treatments . . . . .	37
12	Simulated Superalloy Disk Cross Section for Shock Wave TMP . .	41
13	Photograph of Simulated Superalloy Disk Assembly Before Shock Wave Treatment . . . . .	42
14	Simulated Superalloy Disk, Support Tooling and Explosively Driven Flyer Plate Configuration for 150 Kbar Shock Wave Treatment . . . . .	43
15	Simulated Superalloy Disk after 150 Kbar Shock Wave Treatment and Grit Blasting . . . . .	44

## SECTION I

### INTRODUCTION

The utilization of nickel base superalloys in gas turbine engines is strongly dependent on the capabilities of metallurgical processing techniques. Variations in the process of casting, powder consolidation, deformation, heat treatment and combinations thereof would all be expected to affect the mechanical properties of a particular alloy. Consequently efforts are continually being made to find interrelationships between alloy composition and processing variables that will result in improved high temperature properties for gas turbine engine applications.

The subject of the investigation described herein falls into the above category. Specifically the objective of the research program conducted has been to evaluate the effects of shock wave deformation and thermal treatments (referred to as shock wave TMP) on the microstructure and properties of the nickel base superalloy, AF2-1DA.

The reasons for conducting this study are twofold. First, based on the results of two previous studies conducted by the Denver Research Institute (DRI)<sup>1,2</sup> for Naval Air Systems Command, it was expected that the mechanical properties of AF2-1DA alloy could be improved significantly over that achievable by heat treatment; and second, the use of shock wave techniques introduces the unique ability to deformation process without a shape change. Because of the unusual nature of shock wave processing a review of the important shock wave characteristics and effects is presented in the following section of this report.

Of the two major reasons for conducting this study perhaps the latter (near net shape processing) will have the greatest future significance. Near net shape fabrication concepts have been developed for nickel base superalloy, gas turbine engine components to reduce both material and processing costs. The use of powder metallurgy techniques and/or high temperature isothermal forging are popular approaches to producing near net shape components. However, achieving near net shape by high temperature processing reduces or eliminates the possibility of introducing mechanical deformation which beneficially affects properties of many superalloys in the service temperature range (i.e. 1000°F to 1400°F). It is therefore possible that shock wave deformation processing, with its unique no shape change characteristic, will compliment the hot isostatic pressing, isothermal forging or direct casting processes of producing near net shape gas turbine engine components.

This program has measured the effects of shock wave and thermal treatments on the tensile, stress rupture and fatigue properties of AF2-1DA alloy using wrought plate stock coupons. To demonstrate the potential use of shock wave techniques a 6 inch diameter simulated turbine disk made of steel was shock treated without distortion or damage.

## SECTION II

SHOCK WAVE DEFORMATION

## 2.1 SHOCK WAVES IN METALS

With respect to a solid material a shock wave is a propagating, high pressure disturbance, the magnitude of which is sufficient to cause the material to lose its rigidity and behave in a fluid manner. Such a propagating disturbance is characterized by a sharp discontinuity in pressure, volume and temperature with respect to ambient or initial conditions. The pressure-time profile of a one-dimensional shock wave is illustrated for reference in Figure 1. As the pressure level,  $P$ , increases above the initial condition,  $P_0$  the initial volume,  $V_0$ , will decrease to a new value,  $V$ , and the internal energy of the compressed volume,  $E$ , will be greater than the initial energy,  $E_0$ . Equations relating the change in the state variables, pressure, volume and energy, can be derived by considering the conservation of mass, momentum and energy resulting in the Rankine-Hugoniot relations<sup>3</sup>.

$$1/V(U_s - u_p) = 1/V_0 U_s \quad (1)$$

$$P - P_0 = 1/V_0 U_s u_p \quad (2)$$

$$E - E_0 = 1/2(P + P_0)(V_0 - V) \quad (3)$$

The specific volume is related to the density by

$$V_1 = 1/\rho_1 \quad (4)$$

The velocity with which the compressed state moves into the uncompressed state is called the shock wave velocity,  $U_s$ . The higher the pressure difference the higher will be the shock velocity. In fact the wave velocity is related to the slope of the  $P - V$  curve and expressed as

$$U_s = \left[ \frac{dP}{d(1/V)} \right]^{\frac{1}{2}} \quad (5)$$

For a plane shock wave the material in the compressed region is accelerated to a velocity,  $u_p$ , and referred to as the particle velocity.

The above describes the changes occurring as the uncompressed state is transformed across the shock wave front to the compressed state. The compressed state can, however, be maintained only for a very short period of time (usually on the order of a micro-second or less but depending on the system used to generate the shock wave) and then returns to the initial uncompressed state. The return to the less dense condition which occurs

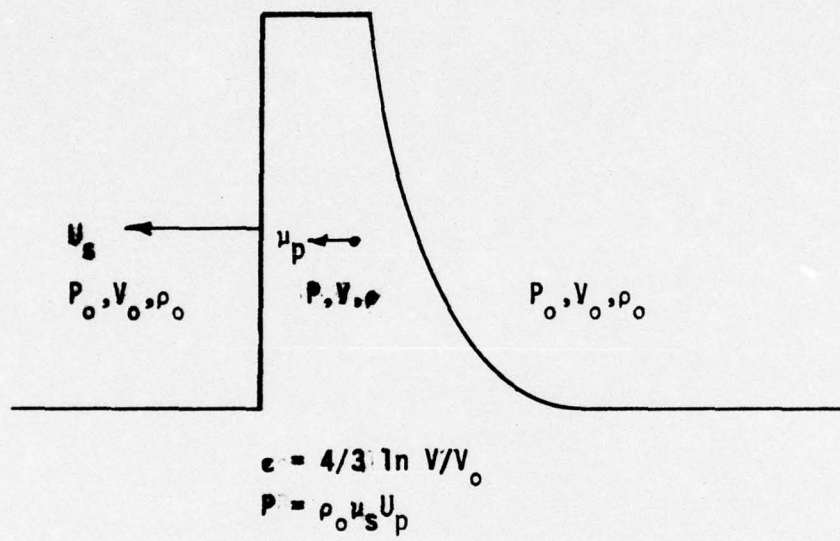


Figure 1. Pressure-Time Profile for One Dimensional Shock.

in a discontinuous manner is referred to as the rarefaction wave. The return to the uncompressed state follows essentially the same path making the process for all practical purposes reversible with respect to the initial and final volume.

The process is not, however, reversible in all respects. A substantial amount of energy must be dissipated during the finite transition time from the uncompressed state to the compressed state and back to the uncompressed state. A certain amount of irreversible plastic work is done on the microstructure of the particular solid subjected to the shock wave. It is this aspect, the modification of microstructure through a reversible volume change, that produces effects similar to that of conventional plastic deformation processes but without the attendant shape change.

A precise description of the atom movements occurring in the shock and rarefaction fronts has not yet been possible. It is possible though to develop a qualitative picture of the transition process and how it might result in an increase in the dislocation density and other effects such as twinning or phase changes.

In a perfect simple cubic lattice the transition from one density state to another must be accompanied by a relative displacement of the atom positions as illustrated in Figure 2. The interface between the two density states must contain dislocations, and the accompanying shear strain will produce a shear stress. This idealized picture was proposed by C. S. Smith<sup>4</sup> in 1958.

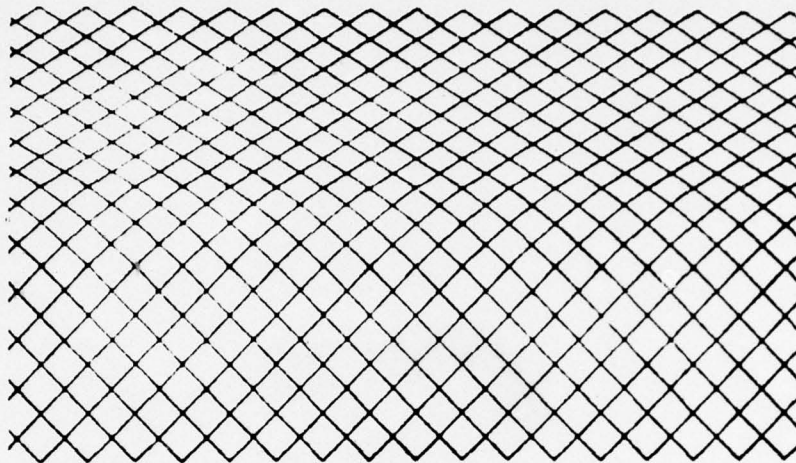
In reality the width of the pressure transition region where dislocations are produced is probably no less than  $10^3$  to  $10^4$  lattice spacings corresponding to a pressure rise time of about 1 nano-second. Experimentally the rise time often appears to be greater than 1 nano-second suggesting a transition width of 10% lattice spacings or greater.

Depending on the magnitude of the pressure and the type of crystal structure, other shear related processes can occur to dissipate energy in the most efficient manner. Examples are the formation of twins in alpha iron, octahedral slip in face centered cubic metals and crystalline phase transformations such as the reversible alpha-epsilon transformation in iron at 133 Kbars.

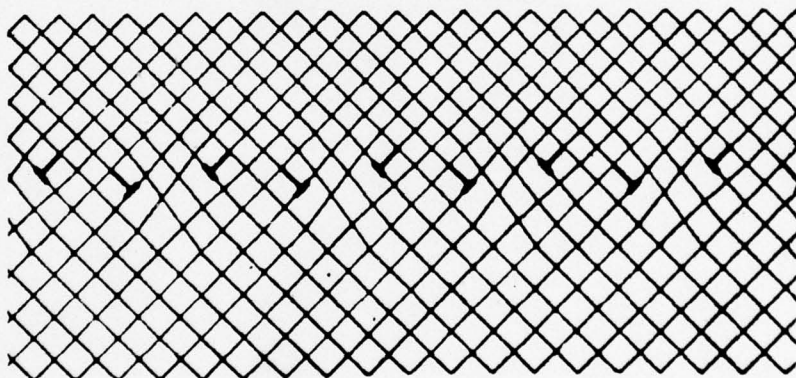
Based on the above description of the production of lattice defects it should be clear that effective shock wave deformation is not related to the less than 1% permanent shape change that can result from the passage of a shock wave. The measure of effective deformation due to shock wave passage must be related to the reversible volume change which is responsible for introducing lattice defects and other changes. Equations relating volume change and effective strain are presented in III, 3.3.

## 2.2 SHOCK WAVE EFFECTS

It was known before 1960 that an explosively induced shock wave of



(a) Uniaxial Distortion of Lattice



(b) Hydrostatic Compression

Figure 2. Relative Displacement of Atoms in a Cubic Lattice Due to Planar Shock Wave.

sufficient magnitude can substantially increase the hardness of most metals and alloys. This effect has been called shock hardening and has come to imply the use of a shock wave to raise the hardness of an annealed metal without the use of pre or post shock heat treatments. Typically shock hardening not only raises the strength and hardness of a metal but lowers the ductility. In ferrite steels the loss of ductility and corresponding increase in brittle behavior can be of a greater magnitude than the increase in strength and hardness. As a result of brittle behavior exhibited by some ferritic steels after shock hardening, the process has been thought of as being detrimental to metal properties in general. This undeserved label has probably been a barrier to the acceptance of shock hardening as a deformation strengthening process.

In spite of the bad publicity, shock hardening has been used commercially since about 1961 in the U.S. It was recognized before 1960 that Hadfield manganese steel castings could be shock hardened without a shape change; the hardened casting yielding substantial improvements in wear life. This process was employed to harden Hadfield manganese, railroad track, switch components (frogs) in 1961 on the Baltimore and Ohio Railroad and continues to be used by the B & O today<sup>5</sup>. The process of shock hardening railroad "frogs" is now being used at several locations in the U.S. and is extensively used in Canada and the Soviet Union<sup>6,7</sup>.

Following the early success of shock hardening many investigations have been conducted during the past 15 years to determine the shock wave response of many metals and alloys. Most of the studies have dealt with the effect of shock waves of varying magnitude on the hardness, micro-structure and sub-structure of both metals and alloys. A summary of shock wave effects in metals follows.

Shock wave deformation tends to be more homogeneous and isotropic than conventional deformation in three respects. First, only the small residual strains (<1%) will lead to any changes in grain shape and long range lattice rotations. In compliance with the small residual strains, texturing and other forms of directional strengthening are minimal<sup>8</sup>. Secondly, the strain through the workpiece thickness is macroscopically uniform, unlike that which normally accompanies the reduction of thicker sections by rolling. As a consequence the section size limitations inherent to certain conventional TMP operations could be overcome by utilizing shock TMP. In fact a shock loading study of 1 inch thick 7075 aluminum alloy for TMP purposes was performed at the Denver Research Institute and at Battelle Memorial Institute<sup>9</sup>. Third, shock wave induced substructures are generally observed to be of a smaller size and more uniformly distributed than that of conventional strain rate deformation<sup>10,11</sup>. This factor affects the strengthening by reducing the mean free path for dislocation motion, or slip-band length; a dependence characterized by  $k$  in the Hall-Petch relation<sup>12</sup>.

The fine scale of shock induced substructure is a consequence of the very high strain rates ( $10^6$ - $10^8$  per sec) at the shock and rarefaction fronts.

The requirement to accommodate an appreciable volume change in a time on the order of  $10^{-9}$  sec. dictates that a high density of dislocations move only a short distance. The result is often the observation of a higher dislocation density than for an equivalent amount of quasi-static plastic deformation<sup>10,11</sup>.

The high rate of deformation in a shock wave also leads to the enhanced generation of vacancies, as predicted by Weertman<sup>13</sup> and confirmed experimentally by Kressel and Brown<sup>14</sup>. Higher vacancy concentration can serve to reduce aging times in precipitation-strengthened systems.

In order to demonstrate that the favorable effect of shock TMP on the properties of nickel base superalloys is neither unique nor an artifact, results of shock TMP in other alloy systems is briefly reviewed. The earliest published account of studies devoted specifically to the modification of properties by combined shock wave and thermal treatments appears to be that of Stein and Johnson in 1963<sup>15</sup>. Their work disclosed the beneficial effect of shock-ausworking and of shock-tempering on the tensile properties of an Fe-3Cr-.4C steel. The technical report by Silverman et al.<sup>16</sup> demonstrated the favorable aspects of shock-tempering on the tensile strength of H-11 and Fe-25Ni steels. In 1964 Koepke et al.<sup>17</sup> illustrated the strength gains attainable by shock-aging A-286 stainless steel, but it was not shown whether conventional deformation would serve the same purpose. This was followed by an investigation by Doherty et al.<sup>18,19</sup> on a number of steels which were shocked and tempered. The primary objective of the program was to demonstrate that irregular shapes could be hardened effectively by utilizing explosives in contact with the workpiece. Again shock-tempering proved to be an effective strengthening technique for H-11 and 4340 steels. However, the results on H-11 did not compare favorably with those of Silverman et al.<sup>16</sup>. This difference can be attributed to the fact that the former investigators shock loaded their material in the solution treated condition while the latter applied a tempering treatment prior to shock wave deformation. Consequently, two aspects of the above mentioned work are particularly significant as far as the present investigation is concerned.

First, irregularly shaped components having little ductility were strengthened by shock waves introduced by explosives without structural damage. And second, there exists an indication that it may be important to establish some form of precipitate before working.

Further evidence of the importance of establishing a precipitate on the microstructure stability at elevated temperature was obtained by the author<sup>20</sup> for 6061-0 and 6061-T6 aluminum. An enhanced stability of the microstructure after shocking to about 25 Kbars was reflected in a 50% higher tensile strength after annealing at 650°F and 775°F when compared to undeformed control material subjected to the same thermal treatment. This was attributed to a very fine three-dimensional network of precipitate ribbons not unlike a network of widely extended dislocations in appearance.

These and other studies indicate the synergistic effects resulting from the interaction of shock wave produced dislocations and micro-structure

which when combined with post shock thermal treatments result in unique new microstructures and in some instances superior mechanical properties.

## SECTION III

EXPERIMENTAL DETAILS

## 3.1 MATERIAL

The AF2-1DA alloy for this investigation was purchased from Universal-Cyclops, Specialty Steel Division. The alloy was in the form of 1/8 inch (.318 cm) thick by 4.0 inch (10.16 cm) wide strips approximately 29 inches (73.7 cm) in length. The alloy strips were produced by hot rolling, straightening, and grinding to the final surface condition. Prior to surface grinding the alloy was annealed at 1950°F for 15 minutes and water quenched. The chemical composition of the alloy heat used to produce the strip stock is quoted from the Cyclops Test Report and is shown in Table 1. The composition listed in Table 1 is within the limits expected for AF2-1DA alloy at the time the material was purchased in April 1974.  
(Heat Number - K70162k11)

Table 1

Chemical Composition of AF2-1DA Alloy (Weight Percent)

Ni	Cr	Co	W	Al	Ti	Mo	Ta	Fe
Balance	12.16	9.96	6.15	4.57	3.02	3.02	1.65	.35
Zr	Mn	C	B	Si	S	P		
.12	.02	.34	.014	.04	.003	.001		

The recommended heat treatment for AF2-1DA alloy to develop optimum properties is the following.

Solution Treatment: 2150°F/2h, Rapid Air Cool(RAC)  
 Intermediate Heat Treatment: 1950°F/2h, Rapid Air Cool(RAC)  
 Final Aging Treatment: 1400°F/16 hr, Air Cool (AC)

The solution treated and aged condition will be referred to as, STA. During the course of the present program all heat treatments were conducted in an argon atmosphere and RAC was accomplished by impinging a stream of argon on the hot plate. Using this technique, cooling from the 2100°F temperature range to 1000°F could be accomplished in 5 to 7 minutes.

In the STA condition the following mechanical properties are quoted by the supplier as typical at 1400°F.

0.2% YS	131.9 ksi (909.4 Mn/m <sup>2</sup> )
UTS	158.7 ksi (1094.2 Mn/m <sup>2</sup> )
Elong.	13.7%

85 ksi (586.1 Mn/m<sup>2</sup>) Rupture Life - 130.9 hr.  
 85 ksi (586.1 Mn/m<sup>2</sup>) Rupture Elong. - 6.8%

### 3.2 PHYSICAL METALLURGY OF AF2-1DA

At the beginning of the program an effort was made to understand the physical metallurgy of AF2-1DA. Based on a report by Buzzanell and Black<sup>21</sup> the precipitation strengthening mechanisms in AF2-1DA appear to be similar to U-700 alloy. Unfortunately, the Buzzanell and Black report as well as other published literature provide little information on the nature of the microstructure and its relation to mechanical properties in the solution treated and intermediate aged conditions. However, the following is thought to represent a reasonably accurate comparison of U-700 and AF2-1DA physical metallurgy.

Both U-700 and AF2-1DA alloys are precipitation strengthened by  $\text{Ni}_3(\text{Al},\text{Ti})$ , an ordered phase with FCC(L1<sub>2</sub>) structure commonly labeled  $\gamma'$ . The precipitate phase is thought to have a low coherency strain with respect to the FCC matrix. This is consistent with the cuboidal morphology exhibited by the precipitate, and its indifference to high strain energy sites such as grain boundaries and deformation induced dislocation arrays. The differences between U-700 and AF2-1DA would appear, therefore, to relate primarily to the higher Ta + W content as well as higher C content. The increase in Ta + W, at the expense of Cr and Co, would be expected to produce greater high temperature solid solution (matrix) strengthening. The high carbon content leads to MC carbide formation which does not benefit AF2-1DA properties, at least below 1500°F. In fact the formation of MC carbide stringers in the rolled plate stock will be shown to have produced erratic test results, a matter discussed in the RESULTS and DISCUSSION section of this report.

At the beginning of the program it was necessary to conduct a series of experiments to evaluate the response of AF2-1DA alloy to solution treatment, cooling rate, and intermediate aging temperature. This was necessary because of the limited amount of such information available in the published literature.

Samples of AF2-1DA alloy were solution treated at 2150°F for 2 hrs. and rapidly cooled (RAC) as described previously. Some of the solution treated samples were intermediate aged at 1950°F for 2 hrs. and RAC. Solution treated (ST) and intermediate aged ( $\gamma'$ ) samples were examined by Scanning Electron Microscope (SEM), including elemental analysis of various phases present in the microstructure. Magnification was 5000X.

The solution treated alloy was found to contain large angular ternary MC carbides of Ta and W. Larger than the MC carbide was an irregular phase, identified as degenerate  $\gamma'$ . The degenerate  $\gamma'$  is thought to be carried through from the as received stock due to incomplete solution treatment. A fine precipitate is distributed uniformly through the matrix and was

identified to be primary  $\gamma'$ . After the 1950°F aging treatment the small  $\gamma'$  precipitate increases in diameter by a factor of 3 or 4 and takes on the characteristic cuboid shape. The MC carbide and degenerate  $\gamma'$  are unaffected by the intermediate aging step.

A second solution heat treatment was performed on AF2-1DA. The solution treatment temperature was raised to 2180°F and again held 2 hours before RAC. Examination of the microstructure after this treatment was found to reduce the degenerate  $\gamma'$  phase to a volume about equal to the MC carbide phase. The MC carbide phase remains unaffected by the increase in solution temperature.

As a result of the degenerate  $\gamma'$  reduction and because the 2180°F/2 hr ST does not appear to increase the grain size, that temperature was chosen to be used for solution treating the AF2-1DA alloy in all remaining processing experiments. Because  $\gamma'$  dissolves at about 2100°F, it may be possible that the furnace temperature is in error and the temperature was actually lower than 2180°F.

Carbide aging experiments were not conducted because some data was available in the literature. According to Collins and Quigg<sup>22</sup>  $M_6C$  carbides are relatively abundant in the microstructure of AF2-1DA alloy after aging at 1950°F for 2 hrs. In the above experiments a fine carbide precipitate phase was observed in the microstructure after the 1950°F/2 hr aging treatment. This phase was not observed in the solution treated microstructure. Presumably the  $M_6C$  carbide abundance is only 1/5 that of the MC carbide and averaging only 1/10 the size.

Dreshfield<sup>23</sup> reports that  $M_{23}C_6$  carbides are very abundant in AF2-1DA after aging at 1600°F for 1500 hrs. No information was given on the relative abundance of  $M_6C$  in AF2-1DA, however,  $M_6C$  was reported to be in medium abundance in AF2-1DA alloy after 1500 hrs at 1600°F. Since  $M_6C$  and  $M_{23}C_6$  carbides do not form at aging temperatures below about 1550°F, we should expect the final (1400°F) aging treatment to have little or no effect on the carbide phase distribution.

In summary we should expect the following carbide phases after the various heat treatment listed

2150°F/2hr	- MC
1950°F/2hr	- MC + $M_6C$
1400°F/16hr	- MC + $M_6C$
2150°F/2hr	- MC
1950°F/2hr	- MC + $M_6C$
1600°F/8hr	- MC + $M_6C$ + $M_{23}C_6$
1400°F/16 hr	- MC + $M_6C$ + $M_{23}C_6$

### 3.3 SHOCK WAVE DEFORMATION OF AF2-1DA

It was expected that AF2-1DA alloy would respond to shock wave deformation

and subsequent heat treatment in a manner similar to U-700 alloy in the previous study because of the similarities in their strengthening mechanisms. As a result a 500 Kbar shock wave pressure having a time duration of approximately 0.5 to 1.0  $\mu$  sec was chosen for the AF2-1DA deformation treatment.

A plane shock wave of approximately 500 Kbar peak pressure was generated in AF2-1DA alloy by the planar impact of a 1/8 inch thick copper driver plate on the specimen assembly. The specimen assembly consisted of a stack of 3 AF2-1DA plates each 1/8 inch (.318 cm) x 4 inch (10.16 cm) x 4 inch (10.16 cm) surrounded by stainless steel spall rails and supported by a 1/4 inch (.635 cm) thick stainless steel spall plate. The stack of AF2-1DA plates was protected from the driver plate impact by a copper plate .040 inch (.10 cm) thick. The entire assembly is held together by epoxy glue. The glue also serves to fill voids and thereby increase acoustic impedance continuity at mating surfaces. A drawing of the shock loading assembly is shown in Figure 3.

The thickness of the driver plate has been calculated to produce a 1  $\mu$ s duration of peak pressure at the front surface of the first specimen in the stack. The pressure pulse should have a square wave characteristic. The peak pressure of 500 Kbar will remain constant through the stack of the 3 AF2-1DA specimens, but the pulse duration will attenuate to about 0.6  $\mu$ s in the last (3rd.) specimen in the stack. The calculation of peak pressure, pulse duration and pulse attenuation has been outlined by Orava and Wittman<sup>24</sup>. A variation in pulse duration between 0.5  $\mu$ s and 1.0  $\mu$ s is not thought to produce a significant variation in dislocation substructure in AF2-1DA. However it is expected that some level of reduced pulse duration, at a constant pressure, will result in a reduction of dislocation substructure<sup>25</sup>. Effect of pulse duration on mechanical properties are thought to occur at less than 1  $\mu$ s.

Shock loading pressures, pulse durations, and volume strain values for this program are based on a calculated Hugoniot equation of state for AF2-1DA alloy. The symbols used in the equations below are presented in Table 2. The method of calculation was discussed in<sup>1</sup> and is based on the atomic fraction summation of equation of state constants for the major elements in the alloy. The assumed equation of state relationship is of the form

$$U_s = C + S u_p \quad (6)$$

When the constants C and S are fractionally summed for the metal elements in AF2-1DA alloy, the following equation results:

$$U_s = 4.750 + 1.419 u_p \quad (7)$$

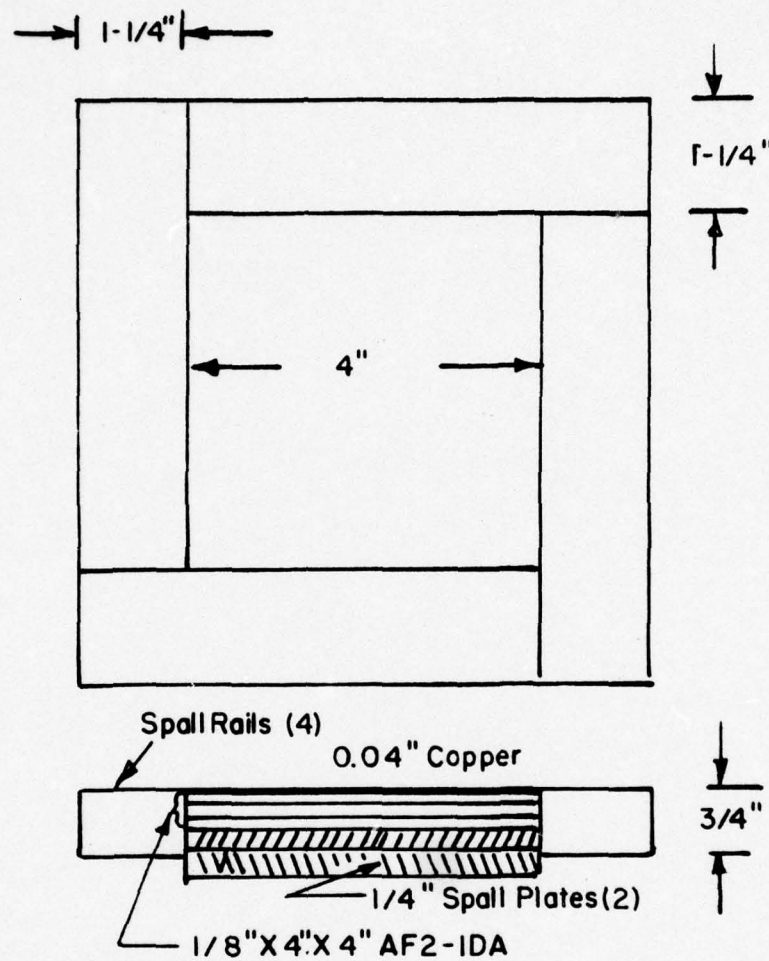
Using the above relationship and 2 other forms of the Hugoniot equation of state,

$$u_p = (1 - \frac{V}{V_0}) U_s \quad (8)$$

$$p = \rho_0 U_s u_p \quad (9)$$

Table 2. Symbols Used in Hugoniot and Shock Relationships

<u>Symbol</u>	<u>Definition</u>
$u_s$	Shock Velocity
$u_p$	Particle Velocity
$\rho_0$	Initial Density
$V_0$	Initial Volume
$V$	Volume at Pressure
$P$	Shock Pressure
$C$	Constant
$\epsilon_s^*$	Effective Shock Strain
$\bar{\epsilon}_v$	True Volume Strain
$\epsilon_v$	Engineering Volume Strain
$\epsilon_r^*$	True Effective Strain, Rolling
$\bar{\epsilon}_{tr}$	True Thickness Strain, Rolling
$\epsilon_{tr}$	Engineering Thickness Strain, Rolling
$\epsilon_{tr}'$	Equivalent Thickness Strain
$\bar{\gamma}_0$	Octahedral Shear Strain
$\epsilon_1$	Strain Normal to Shock
$\epsilon_2$	Strain Parallel to Shock
$\epsilon_3$	Strain Parallel to Shock
$\bar{\gamma}_{os}$	Octahedral Shock Strain
$\bar{\epsilon}_1$	Engineering Strain in Rolling
$\bar{\gamma}_{or}$	Octahedral Rolling Strain
$\bar{\gamma}_m$	Maximum Shear Strain
$\bar{\gamma}_{ms}$	Shock Shear Strain
$\bar{\gamma}_{mr}$	Rolling Shear Strain



Spall plates and rails: 304 Stainless steel

All mating surfaces bonded with epoxy

Figure 3. Configuration of AF2-1DA Sample and Tooling for Shock Wave TMP.

A listing of calculated parameters on the Hugoniot as a function of pressure is presented in Table 3.

A comparison of shock wave deformation to slow strain rate deformation processing conditions can be made on the basis of effective or generalized strain. The appropriate shock wave strain to be used as the basis of comparison is taken as the true transient (effective) shock strain expressed as

$$\bar{\epsilon}_s^* = 4/3 \ln V/V_0 = 4/3 \bar{\epsilon}_v \quad (10)$$

$$\text{or as } \bar{\epsilon}_s^* = 4/3 \left( \frac{V-V_0}{V_0} \right) = 4/3 \epsilon_v \quad (11)$$

in terms of engineering effective shock strain. When  $\bar{\epsilon}_s^*$  from (10) is equated to the true effective strain imparted by rolling,  $\bar{\epsilon}_r^*$ , as given by

$$\bar{\epsilon}_r^* = 2/\sqrt{3} \quad \bar{\epsilon}_{tr} = 2/\sqrt{3} \ln(1 + \epsilon_{tr}) \quad (12)$$

then the thickness strain,  $\epsilon_{tr}'$ , required for equivalence to a given volume strain is given by

$$\epsilon_{tr}' = \exp(2/\sqrt{3} \ln V/V_0) - 1 \quad (13)$$

For example a shock wave pressure of 441 Kbar in AF2-1DA will result in a transient volume reduction of 15% ( $V/V_0 = 0.85$ ) or a true effective shock strain,  $\bar{\epsilon}_s^*$  of -0.217. From 13 the equivalent thickness strain,  $\epsilon_{tr}'$ , imparted by rolling would be -0.171. Strain equivalents for other deformation methods can be derived in a similar manner.

Another strain invariant function which could be used for comparison of shock wave deformation to conventional deformation is the octahedral shear strain, normally expressed as a matrix strain rather than a tensor value. Thus

$$\bar{\gamma}_0 = 2/3 [(\bar{\epsilon}_1 - \bar{\epsilon}_2)^2 + (\bar{\epsilon}_2 - \bar{\epsilon}_3)^2 + (\bar{\epsilon}_3 - \bar{\epsilon}_1)^2]^{1/2} \quad (14)$$

Assuming that planar shock compression results in a uniaxial strain state ( $\bar{\epsilon}_1 = 4/3 \ln V/V_0$ ,  $\bar{\epsilon}_2 = \bar{\epsilon}_3 = 0$ ), then the octahedral shear strain due to a shock wave is

$$\bar{\gamma}_{os} = \frac{4\sqrt{2}}{3} \ln V/V_0. \quad (15)$$

For rolling deformation  $\bar{\epsilon}_1 = \bar{\epsilon}_{tr} = -\bar{\epsilon}_2$  and  $\bar{\epsilon}_3 = 0$ , which when substituted in (14) results

$$\bar{\gamma}_{or} = \frac{2\sqrt{2}}{\sqrt{3}} \quad \bar{\epsilon}_{tr} = \frac{2\sqrt{2}}{\sqrt{3}} \ln(1 + \epsilon_{tr}). \quad (16)$$

Table 3  
Calculated Hugoniot Parameters for AF2-TDA

$C_0$  = Bulk Sound Velocity = 4750m/s

$\rho_0$  = Initial Density = 8.083 g/cm<sup>3</sup>

$V_0$  = Initial Volume = 1/ $\rho_0$

P Kbar	$\rho$ g/cm <sup>3</sup>	V/V <sub>0</sub>	U <sub>s</sub> m/s	U <sub>p</sub> m/s	C m/s
0	$\rho_0$	1.0000	$C_0$	0	$C_0$
50	8.294	0.9745	4928	126	4975
100	8.488	0.9523	5095	243	5177
150	8.666	0.9327	5251	353	5361
200	8.832	0.9152	5397	456	5528
250	8.988	0.8993	5542	558	5688
300	9.135	0.8849	5678	654	5836
350	9.273	0.8716	5808	746	5975
400	9.405	0.8594	5933	834	6107
450	9.530	0.8481	6055	919	6233
500	9.650	0.8376	6172	1002	6353
550	9.764	0.8278	6286	1082	6468
600	9.874	0.8186	6397	1160	6578

The maximum shear strain experienced by the deformed metal is given by

$$\bar{\gamma}_m = \bar{\epsilon}_{max} - \bar{\epsilon}_{min} \quad (17)$$

Since  $\epsilon_2 = \epsilon_3 = 0$  for the shock wave case, then

$$\bar{\gamma}_{ms} = \bar{\epsilon}_1 = 2 \ln V/V_0 \quad (18)$$

For the rolled condition,

$$\bar{\gamma}_{mr} = 2 \bar{\epsilon}_{tr} = 2 \ln(1 + \epsilon_{tr}) \quad (19)$$

The magnitude of the various pressure and strain parameters is given in Table 4 for AF2-1DA alloy.

Table 4

## Pressure, Volume and Equivalent Strain Parameters for AF2-1DA Alloy

Shock Pressure (Kbar)	500
$V/V_0$ at 500 Kbar	0.8376
$\epsilon_v = \frac{V-V_0}{V_0}$	-0.1624
$\bar{\epsilon}_v = \ln V/V_0$	-0.1772
$\epsilon_s^* = 4/3 \epsilon_v$	-0.2165
$\bar{\epsilon}_s^* = 4/3 \bar{\epsilon}_v$	-0.2362
Equivalent Thickness Strain by Rolling, $\epsilon_{tr}^1$	- .1851
$\bar{\gamma}_{os}$	- .3341
$\bar{\gamma}_{ms}$	- .3544
Equivalent Maximum Shear Strain by Rolling, $\bar{\gamma}_{mr}$	- .4094

## 3.4 SHOCK WAVE TREATMENT PROCEDURE

Shock wave treatment of the AF2-1DA specimen assembly illustrated in Figure 1 was accomplished by explosively propelling a 1/8 inch thick copper driver plate to a predetermined velocity. The copper driver plate is propelled so that impact occurs simultaneously over the entire surface, a collision mode usually referred to as a planar impact. A drawing of the shock wave apparatus is shown in Figure 4.

The impact velocity required of the copper driver plate to produce a 500 Kbar pressure in the stationary target (specimen assembly) is calculated using the reflection Hugoniot techniques described by Duvall<sup>26</sup>. For this procedure it is necessary to have Hugoniot equation of state data in a pressure-particle velocity format.

To develop a 500 Kbar shock wave in AF2-1DA alloy using a copper driver plate the impact velocity is calculated to be 2026 m/s. Using this calculated impact velocity it was then possible to determine the required explosive loading and initial separation of driver plate and target assembly.

The model used to calculate the impact velocity of the driver plate is that developed by Gurney<sup>27</sup> in 1943. Subsequent modifications based

on gas dynamics have confirmed the validity of the Gurney model in the velocity range of interest<sup>28,29,30</sup>. The Gurney equation for the untamped, explosive/metal combination is

$$V_p = \sqrt{2E} \left( \frac{3}{1 + 5(m/c) + 4(m/c)^2} \right)^{\frac{1}{2}} \quad (20)$$

where  $V_p$  is the steady-state or maximum velocity of the driver plate;  $E$  is the specific or "Gurney energy" of the explosive;  $m$  is the mass of the driver plate per unit area; and  $c$  is the mass of explosive per unit area.

The explosive used during this program was du Pont's E1-506C, Datasheet, a flexible sheet explosive composition. The specific "Gurney velocity",  $\sqrt{2E}$ , for Datasheet using the plane wave configuration has been found to be approximately 2990 m/s. The 1/8 inch thick copper driver plate has an areal density,  $m$ , of 2.83 g/cm<sup>2</sup>. Substituting  $m$ ,  $\sqrt{2E}$  and  $V_p$  in (20), a value for  $c$  can be determined. The value of  $c$ , using Datasheet explosive, to produce a flyer velocity of 2026 m/s is 3.99 g/cm<sup>2</sup>. The Datasheet explosive for this program was available in sheets having loadings of .31 g/cm<sup>2</sup> and .62 g/cm<sup>2</sup>. Using various integer multiples of those loadings it was necessary to choose an explosive loading of 4.03 g/cm<sup>2</sup> or 13 layers of the .31 g/cm<sup>2</sup> Datasheet to satisfy or exceed the minimum requirement. The expected impact velocity,  $V_p$  from the increased loading would be 2036 m/s; an increase of only 10 m/s. The increase in shock wave pressure would be no more than 1 Kbar. The values are insignificant when compared to an expected uncertainty in the impact velocity due to all causes of  $\pm 5\%$ .

The explosive charge must be simultaneously initiated over the surface opposite the flyer plate in order to produce a planar impact and shock wave in the target assembly. The explosive "mousetrap" technique was used in this study to achieve simultaneous initiation. The mousetrap configuration is shown in Figure 4. The Datasheet explosive on the glass plate is line initiated using a du Pont line wave generator. The propagation of the explosion front over the glass propels glass fragments across the gap to strike the surface of the main charge. The high velocity impact of the glass fragments initiates the main charge. The angle of inclination of the glass plate is set so that glass fragments impinge simultaneously and therefore initiate simultaneously.

The Gurney model applies only to the prediction of a maximum driver plate velocity and does not describe the acceleration history. It is necessary to use a standoff between flyer plate and target that will allow acceleration to maximum velocity. The minimum distance can be estimated as 0.2 times the thickness of the explosive plus driver plate. The explosive plus driver plate thickness was 1.2 inches (3.05 cm) for the 13 layers of explosive and 1/8 inch (0.32 cm) copper driver plate. The minimum standoff for this combination would be 0.24 inches (0.61 cm). However, to insure a sufficient acceleration distance the standoff was increased to 3/8 inch (.95 cm).

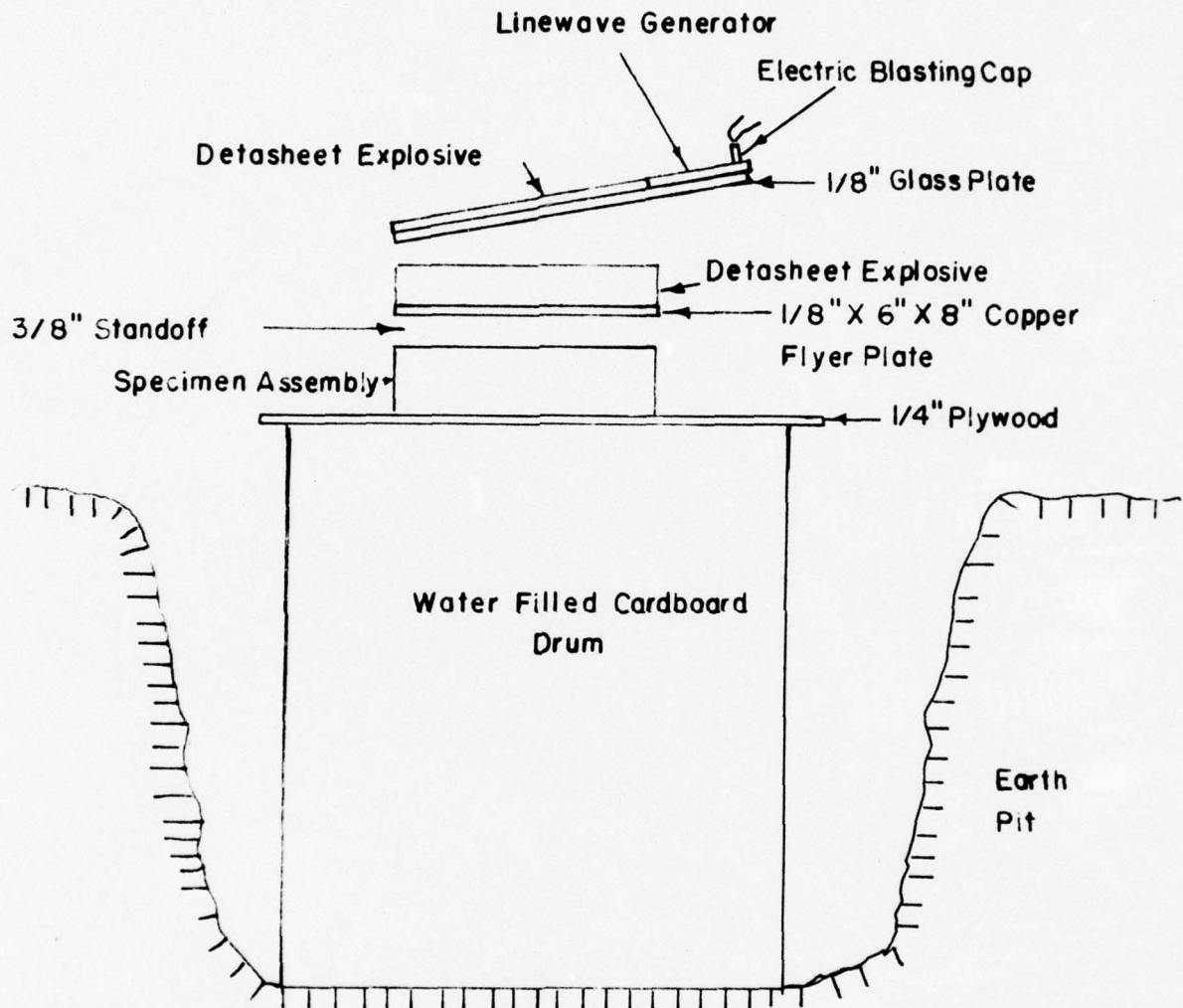


Figure 4. Configuration of Explosive-Flyer Plate Assembly, Specimen Assembly and Recovery Pit for Shock Wave TMP of AF2-1DA.

### 3.5 MECHANICAL TESTING PROCEDURE

Tensile tests at all temperatures were conducted in air with a floor model 10,000 lb capacity Instron testing machine at a strain rate of  $2.8 \times 10^{-4}$  per sec (crosshead speed = 0.02 in/min). Elevated temperatures were controlled by means of a chromel-alumel thermocouple positioned close to the reduced gage section of the tensile specimen. Tensile specimens were cut from the AF2-1DA plates with the tensile axis parallel to rolling direction. Because of the extreme hardness of the shock processed plates it was necessary to use special techniques to produce not only the tensile specimens but also the stress-rupture and low-cycle fatigue specimens. The basic specimen shape was electrically discharge machined (EDM). Final dimensions were achieved by grinding, including notches and pin holes. A drawing of the tensile specimen design is shown in Figure 5. A load time record was obtained for each test specimen from which various stress parameters were determined. Final area at fracture was measured using an optical comparator.

Stress-rupture life and elongation were evaluated at constant load by means of a Satec creep machine. Temperature was monitored by means of a thermocouple placed near the specimen surface and controlled to  $\pm 3^\circ\text{F}$ . Specimen elongation was monitored as a function of time using a dial indicator capable of detecting displacements of  $2 \times 10^{-5}$  inches ( $5.08 \times 10^{-5}$  cm). Since the dial indicator is mounted outside the furnace on the loading beam, the reading reflects both machine and specimen displacements. To minimize this effect the dial indicator is set to zero after the specimen has been loaded at temperature. Under constant load only the reduced section of the specimen would be expected to undergo continued displacement. Assuming elastic strains are negligible, the measured displacements can be taken to correspond to plastic extension of the sample in the reduced gage section. Creep curves were obtained by plotting the percent elongation against time. The specimen design was the same as the tensile specimen shown in Figure 5.

Low-cycle notched fatigue tests were performed in an Instron testing machine by stress cycling in a tension-tension mode at a frequency of 2 cycles per minute (0.03 Hz). Tension fatigue specimens were a flat, double-edge notched design shown in Figure 6. The notches were ground and measured for accuracy using an optical comparator. The notch design was chosen to develop a stress concentration factor of  $K_t = 3.0 \pm 12^{25} 31$ .

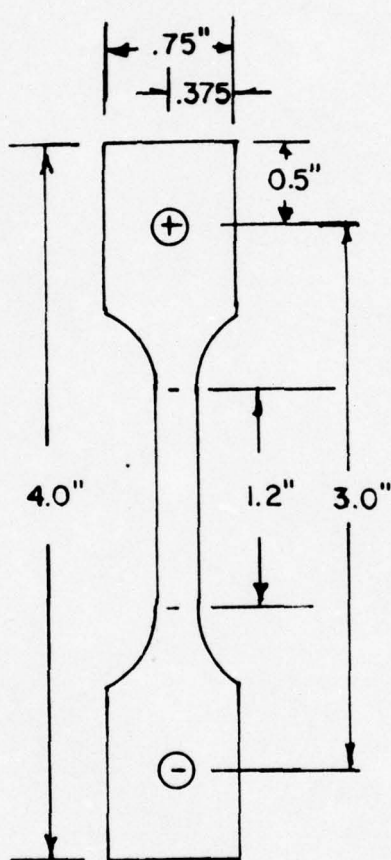


Figure 5. AF2-1DA Tensile and Stress Rupture Specimen Design.

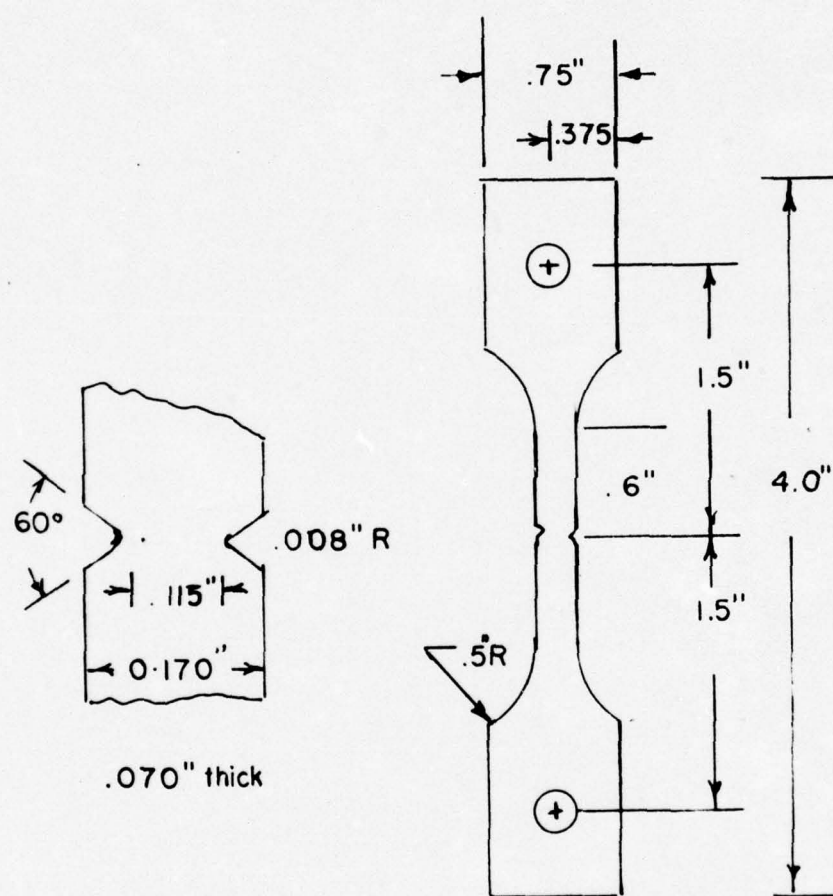


Figure 6. AF2-1DA Low Cycle Tension-Fatigue Specimen Design.

## SECTION IV

RESULTS AND DISCUSSION

Experiments were conducted with the objective of comparing the properties of AF2-1DA alloy in the STA condition to various shock wave thermomechanically processed (TMP) conditions. An attempt was made to introduce an equivalent amount of rolling deformation at room temperature in order to provide a comparison to the shock wave TMP condition. However, cracking always resulted before the necessary thickness reduction of 18% could be obtained. Conventional strain rate TMP attempts were therefore abandoned because of the extreme strength of AF2-1DA and lack of ductility at low and intermediate temperatures.

## 4.1 TENSILE PROPERTIES OF AF2-1DA

Initial experiments were aimed at determining the tensile properties of the AF2-1DA alloy plate in the STA condition as well as intermediate aged condition in order to establish a basis for comparison with shocked samples. The room temperature, 1400°F and 1500°F tensile properties for the DRI heat treated alloy are listed in Table 5. In addition the room temperature tensile properties for the intermediate aged ( $\gamma'$ ) condition are presented in Table 5. Cyclops data for comparable heat treatment and test conditions are also listed.

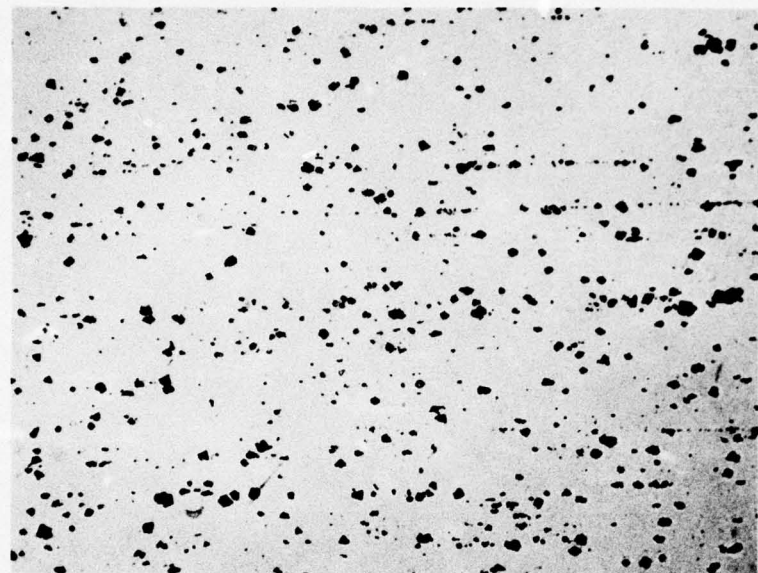
Inspection of the data in Table 5 indicates that duplication of the room temperature (RT) and 1400°F tensile properties reported by Cyclops was not achieved. This was particularly evident in a comparison of the (RT) properties. The Cyclops data shows a greater work hardening behavior as evidenced by the lower yield strength, higher tensile strength (UTS) and lower elongation. Examination of the microstructure (Figure 7) of the processed AF2-1DA reveals what might be an abnormally high MC carbide content. Estimation of the MC carbide content by quantitative metallographic means establishes the weight percent as 2.5-3.6 for the STA condition. The carbide distribution was not entirely uniform from location to location, the reason for the range in the reported weight percent. Reference 21 reports an MC carbide range of 1.0 to 2.9 weight percent for AF2-1DA, significantly lower than determined for the material used in this study. It would be reasonable to expect the higher carbide content to raise the yield strength and reduce the work hardening rate. The lowered UTS could also be attributed to the higher carbide content; carbides initiating crack propagation and rupture at lower stress values. The tensile elongations are not significantly different. Elongation differences of 1% may result from comparing specimens of different gage length. In addition the elongation measurements are more subject to error than the yield and UTS values. An elongation of 1% represents only 0.012 inches in the DRI specimens. The differences are less pronounced at 1400°F.

The yield and UTS are within the variation that might be expected at 1400°F; however, the elongation of the DRI tested AF2-1DA was low by comparison. In this case the low elongation could reasonably correlate to

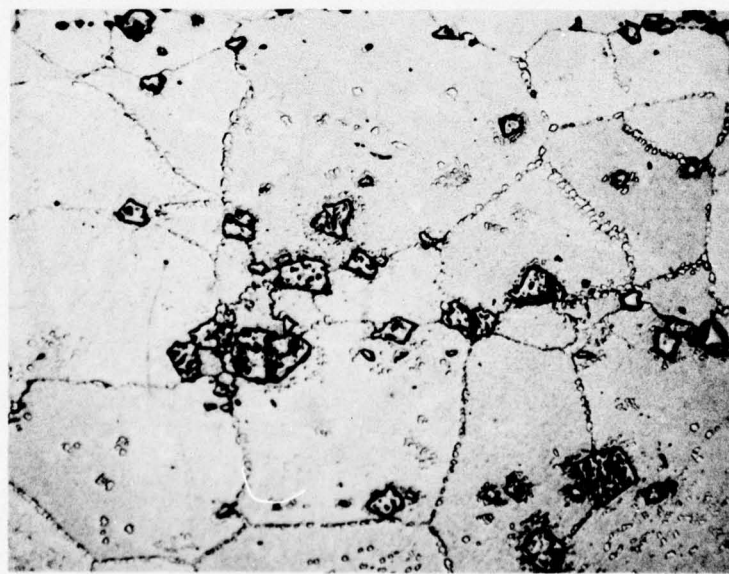
Table 5. Room and Elevated Temperature Tensile Properties of AF2-1DA in the STA Condition

Specimen Condition	Test Temp.	0.2%YS (Ksi)	UTS (Ksi)	Elong. (%)	R.A. (%)	Room Temp. Hardness, RC	Remarks
ST+ $\gamma'$ +F	Room	132.9	176.7	12.6	9.7	43.8	
"	"	136.5	173.9	12.8	10.9	43.0	
"	"	134.4	177.6	13.3	13.0	43.8	
"	"	(134.6)	(176.1)	(12.9)	(11.2)	(43.5)	Average
"	"	130.2	195.7	11.5	-	-	Ref. 21 Table XLV
ST+ $\gamma'$ +F	1400°F	130.0	160.0	12.1	-	-	Ref. 21 Table XLV
"	"	131.9	158.7	13.7	-	-	Cyclops Typical
"	"	133.1	159.5	9.2	11.1	43.3	
"	"	135.1	162.4	10.5	11.2	44.2	
"	"	(134.1)	(161.0)	(9.9)	(11.15)	(43.8)	Average
ST+ $\gamma'$ +F	1500°F	104.5	134.00	12.5	-	-	Ref. 21
ST+ $\gamma'$	Room	120.5	185.3	11.7	10.0	42.8	
"	"	127.2	167.0	13.8	12.0	41.5	
"	"	(123.9)	(176.2)	(12.8)	(11.0)	(42.2)	Average

ST - Solution Treated-2180°F/2hr-RAC  
 $\gamma'$  - Gamma Prime Age-1950°F/2hr-RAC  
 F - Final Age-1400°F/16hr-AC



100X



500X

Figure 7. Typical AF2-1DA Alloy Microstructures after STA Processing. Carbide Stringers of the Magnitude Shown in Figures 7 and 10 were not Observed at the Beginning of the Program.

the high carbide content; the carbides serving as crack initiators, reducing the apparent toughness by localizing the flow processes near the final stage of rupture. The RA would be lowered by this type of mechanism; however, in this case typical RA data was not available for comparison. Because the MC carbide content is largely unaffected by heat treatment of a type compatible with other desirable characteristics (i.e., fine grain size), nothing was attempted to correct the problem and the work proceeded as planned.

#### 4.2 TENSILE PROPERTIES OF AF2-1DA AFTER SHOCK WAVE TMP

The response of U-700 alloy to shock wave TMP in the previous program<sup>2</sup> indicated one of the best conditions involved shock wave deformation after the  $\gamma'$  aging sequence. In this case the precipitate is thought to interact with dislocations resulting in both a finely distributed dislocation structure in the matrix and effective deformation of the  $\gamma'$ . Subsequent aging at 1400°F does not destroy the beneficial effect of the dislocation substructure introduced. A comparable response was postulated for AF2-1DA because of the structural similarities.

Shock wave TMP experiments were designed to introduce the shock wave strain after  $\gamma'$  aging but prior to the final aging. Therefore it was necessary to determine the influence of  $\gamma'$  particle size and spacing on the degree of shock strengthening. The  $\gamma'$  particle size and spacing is controlled by the temperature of the  $\gamma'$  aging treatment. The effects of three  $\gamma'$  aging temperatures, 1900°F, 1950°F and 2000°F, were evaluated. In each case the aging time was 2 hours followed by RAC. The shock wave pressure was 500 Kbar in each case and the final aging temperature was 1400°F for 16 hours. Tensile testing for these 3 conditions was conducted at room temperature and 1400°F for comparison to the STA condition. Selected samples were also tested at 1500°F. The results are listed in Table 6, and tensile properties as a function of testing temperature are graphically displayed in Figure 8.

Examination of the tensile test results listed in Table 6 reveal many interesting comparisons. Perhaps the most significant result is the identification of a  $\gamma'$  aging temperature (1900°F) prior to shock wave treatment and final aging that results in tensile properties at 1400°F and 1500°F superior to the STA condition at the same temperatures. For example at 1400°F the 0.2% yield strength average is 17% greater than the Cyclops typical value and 15% greater than the yield strength of the STA condition measured in this program. The UTS value for the shock treated AF2-1DA is only slightly higher than for the STA condition at the 1400°F temperature. The ductility values for the shock treated and STA conditions are essentially equal at the 1400°F test temperature. Even more impressive are the yield and UTS increases for the shock treated AF2-1DA at 1500°F. The yield and UTS is greater than the STA condition at 1500°F by 19.5% and 6.8% respectively. At room temperature the yield and UTS of the shock TMP material is respectively 44% and 30.7% higher than the typical STA properties. The ductility parameters are, however, significantly reduced.

What is the explanation for these results? The fact that yield strength increases are greater than UTS increases at all temperatures would

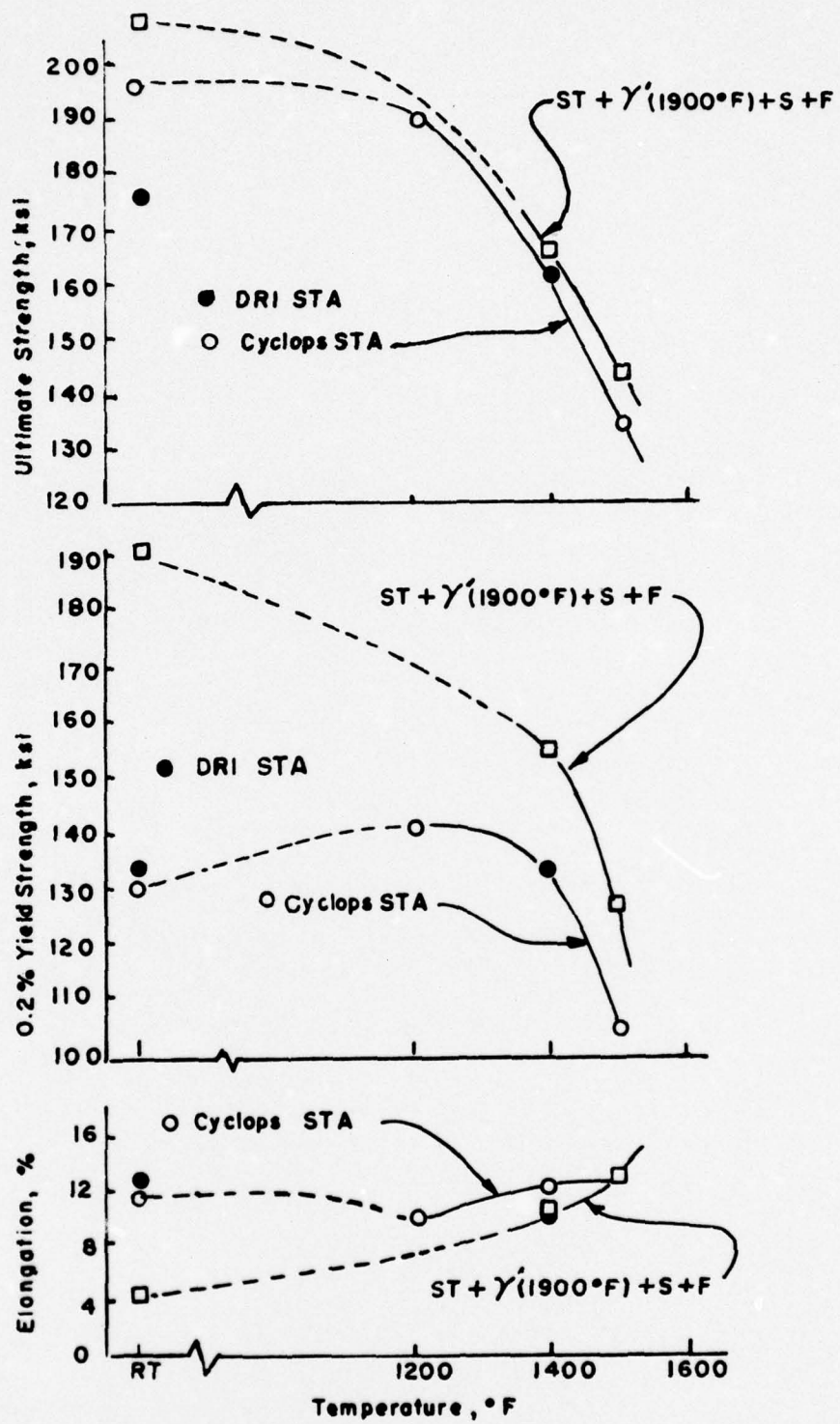


Figure 8. Tensile Properties of AF2-1DA Alloy after Various Treatments.

Table 6. Room and Elevated Temperature Tensile Properties of AF2-1DA after Shock-wave TMP

Specimen Condition	Test Temp.	0.2%YS (Ksi)	UTS (Ksi)	Elong. (%)	R.A. (%)	Room Temp. Hardness, Rc	Remarks
ST+ $\gamma'$ +F(STA)	1400°F	131.9	158.7	13.7	-	-	Cyclops Typical
"	"	134.1	161.0	9.9	11.2	43.8	Average This Program
"	1500°F	104.5	134.0	12.5	-	-	Ref 21
ST+ $\gamma'$ (1900°F)	1400°F	152.6	164.5	11.7	15.0	48.2	
"	"	156.3	168.1	9.5	11.9	49.7	
"	"	(154.5)	(166.3)	(10.6)	(13.5)	(48.9)	Average
"	1500°F	124.9	143.1	13.2	15.1	50.4	
ST+ $\gamma'$ (1950°F)	1400°F	145.2	157.3	5.7	8.3	48.7	
"	"	141.2	163.2	11.7	16.9	48.6	
"	"	(143.2)	(160.3)	(8.7)	(12.6)	(48.7)	Average
ST+ $\gamma'$ (2000°F)	1400°F	152.1	164.8	4.1	6.4	47.8	
"	"	148.9	170.1	5.0	8.3	48.3	
"	"	(150.5)	(167.5)	(4.5)	(7.4)	(48.0)	Average
ST+ $\gamma'$ (2000°F)	1500°F	117.5	132.6	2.4	2.1	49.0	
ST+ $\gamma'$ +F(STA)	Room	130.2	195.7	11.5	-	-	Ref 21 Table LV
ST+ $\gamma'$ (1900°F)	Room	184.7	200.5	3.3	3.1	49.8	
"	"	196.5	214.3	4.6	4.2	50.6	
"	"	(190.6)	(207.4)	(4.0)	(3.7)	(50.2)	Average
ST	- Solution Treated-2180°F/2hr-RAC				S	- Shock Wave Deformation-500Kbar	
$\gamma'$ (temp.)	- Gamma Prime Age-2hr-RAC				F	- Final Age-1400°F/16hr-AC	

indicate the shock wave deformation has introduced a significant density of dislocation substructure in the matrix that is stable for short time temperature exposures to 1500°F. The yield strength is raised by the dislocation structure, and the stability of the structure is probably the result of the secondary  $\gamma'$  (final age at 1400°F) and possibly to the rearrangement and formation of a more stable dislocation network. As is typical with dislocation strengthening (cold work hardening) the UTS is not increased to the same extent as the yield strength. The fact that a 1900°F intermediate aging temperature is more effective than the standard 1950°F or a 2000°F aging temperature is an indication of the importance of  $\gamma'$  size and distribution on the introduction of dislocation structure by shock wave deformation. Perhaps it is possible that a small  $\gamma'$  (1900°F) size can be effectively strain hardened by the high stress available with the shock wave deformation. It is also possible that a smaller  $\gamma'$  coupled with the very high shock stress forces a refinement of slip process in the matrix and results in a more homogeneous deformation. Slip refinement and  $\gamma'$  deformation were reported by Orava<sup>2</sup> for U-700 in the previous study of shock wave TMP effects. The low ductility at 1400°F exhibited by the 2000°F intermediate aging treatment could be the result of a larger  $\gamma'$  size with a larger percentage distributed in the grain boundary, the latter responsible for reduced ductility. It is also important to note the ductility of the higher strength shock TMP material has not been lowered relative to the STA condition at the 1400°F test temperature. It would be reasonable to assume that shock deformation has not resulted in the cracking of MC carbides as is often the case with other forms of deformation.

A second series of shock wave TMP experiments was conducted to determine the effect of shock wave treatment before  $\gamma'$  aging. AF2-1DA alloy plates were shock wave deformed to 500 Kbar in the solution treated condition. After the shock wave treatment the samples were  $\gamma'$  aged at 1950°F for 2 hours and RAC. Final aging at 1400°F for 16 hours followed. Tensile samples were cut from the shocked plates and tensile tested at 1400°F and room temperature. The results are listed in Table 7.

The introduction of shock deformation (500 Kbar) prior to intermediate and final aging does produce a TMP effect although not to the same extent as shocking after intermediate aging. The yield strength average at the 1400°F test temperature was only 4.6% greater than the yield strength for the STA condition at 1400°F measured during the program. The UTS value was essentially the same and the ductility of the shock TMP condition was slightly higher than for the corresponding STA condition. Comparison of the ST+S+ $\gamma'$ (1950°F)+F condition to the ST+ $\gamma'$ (1950°F or 1900°F)+S+F condition shows the former to be inferior in all tensile property categories.

Introducing dislocation structure by shock wave prior to the 1950°F  $\gamma'$  aging cycle is relatively ineffective as a strengthening process. This is probably due to the partial annihilation of dislocation structure at the 1950°F aging temperature which would be expected. The existence of dislocation structure would not be expected to affect the  $\gamma'$  precipitation since the  $\gamma'$  is coherent with the matrix and does not prefer a high energy site. The strengthening that is observed can probably be attributed to the rearrangement of the decreased dislocations density at the 1950°F tem-

Table 7. Tensile Properties of AF2-1DA - Effect of  $\gamma'$  Before Shock Treatment and Effects of Carbide Aging After Heat Treatment

Specimen Condition	Test Temp.	0.2%YS (Ksi)	UTS (Ksi)	Elong. (%)	R.A. (%)	Room Temp. Hardness, Rc	Remarks
ST+S+ $\gamma'$ (1950°F)+F	1400°F	141.6	154.2	9.8	13.1	47.7	
	"	138.9	153.6	10.5	13.2	47.1	
	"	(140.3)	(153.9)	(10.2)	(13.2)	(47.4)	Average
Room	164.1	187.3	6.5	7.3	47.1		
ST+ $\gamma'$ (1900°F)+S+C(1600°F)+F	1400°F	159.1	171.5	5.7	8.3	50.1	
	Room	201.4	218.7	2.0	2.0	50.9	
ST+S+C(1600°F)+F	1400°F	141.0	154.9	14.0	17.1	47.5	
	"	146.9	157.3	14.6	17.1	48.1	
	"	(144.0)	(153.1)	(14.3)	(17.1)	(47.8)	Average
ST+ $\gamma'$ +F(STA)	1400°F	134.1	161.0	9.9	11.2	43.8	Average-Table 5
ST+ $\gamma'$ (1900°F)+S+F	1400°F	154.5	166.3	10.6	13.5	48.9	Average-Table 5

ST - Solution Treated-2180°F/2hr-RAC

$\gamma'$  (Temp.) - Gamma Prime Age-2hr-RAC

C - Carbide Age-1600°F/8hr-AC

F - Final Age-1400°F/16hrAC

S - Shock Wave Deformation-500Kbar

perature into a stable network. The formation of temperature stable dislocation networks has been observed in high stacking fault energy alloys as a result of aging to over 70% of the melting point<sup>9</sup>.

There is also increasing evidence in the results (not appreciated until later in the program) of unknown factors affecting the ductility of the AF2-1DA alloy. The amount of necking observed during tensile testing was often very small. Tensile specimens would fracture at or just past peak load. This would be indicative of a fracture produced by internal cracks becoming critical in size and rapidly propagating perpendicular to the tensile axis. As will be discussed later, large MC carbides were thought to be responsible for just such behavior.

Another shock wave TMP sequence that showed promise during the previous study by Orava<sup>2</sup> involved a carbide age while eliminating the intermediate ( $\gamma'$ ) aging sequence. For the present study a similar treatment was investigated, namely ST+S+C(1600°F/8hr)+F. A stack of AF2-1DA plates in the solution treated condition was shock wave deformed at 500 Kbar. Shock wave treatment was followed by carbide aging at 1600°F for 8 hours and final aging at 1400°F for 16 hours. Tensile samples were prepared and tested at 1400°F. The results are listed in Table 6.

The logic behind the ST+S+C+F TMP cycle is the following. First, rapid air cooling (RAC) from the solution treating (ST) temperature does not completely suppress  $\gamma'$  formation. A very fine  $\gamma'$  is produced during quenching and the purpose of the intermediate aging cycle (1950°F) is to effectively coarsen the  $\gamma'$ , thus increasing the percentage of that phase. The ST+S+C+F TMP sequence is designed to introduce dislocation structure by shocking after solution treatment with the hope that existing  $\gamma'$  will be sufficient to develop the dislocation-particle interactions that seem to be beneficial. Carbide aging (1600°F) is designed to precipitate  $M_{23}C_6$  carbide preferentially on dislocations to achieve additional pinning that should enhance the resistance to plastic flow (i.e., increase the work hardening rate). Often carbide precipitation is detrimental to ductility as it tends to occur at grain boundaries in the absence of other high energy sites. However, it is expected that shock induced dislocation structure will cause a more homogeneous carbide precipitation. Final aging at 1400°F should result in secondary  $\gamma'$  formation in the matrix further increasing the resistance to deformation.

The results of the ST+S+C+F sequence would tend to indicate the above strengthening mechanisms are operative with one exception. Hardness measurements after shock deformation of the ST condition were 50-51  $R_C$ , indicating the introduction of a significant amount of dislocation structure. However, carbide aging at 1600°F causes the hardness to drop to the 45-46  $R_C$  range. Final aging causes the hardness to increase back to the 45-48  $R_C$  range. Based on the significant drop in hardness after shock treatment it would appear the absence of the  $\gamma'$  coarsening treatment adversely affects the stability of the dislocation structure. This same type of hardness response was observed in the ST+S+ $\gamma'$ +F processing schedule where the 1950°F heat treatment followed shock wave treatment. Although the yield and UTS properties of the ST+S+C+F schedule were not what had been anticipated, the ductility was excellent and the yield strength was greater than the STA

condition. The combination of strength and ductility enhancement should increase the toughness. This will in fact be demonstrated in the stress rupture and low cycle fatigue results.

The logical step to improve the ST+S+C+F schedule would be the addition of a  $\gamma'$  coarsening heat treatment prior to shocking. Based on the first series of experiments (Table 5) it would appear the  $\gamma'$  coarsening temperature should be no higher than about 1900°F. Therefore to provide a  $\gamma'$  precipitate to interact with dislocations a 1900°F/2hr/RAC heat treatment was chosen to precede the shock treatment in a process schedule designated ST+ $\gamma'$ +S+C+F.

After solution treating and  $\gamma'$  aging at 1900°F for 2 hr. a stack of 3 plates was shock treated to 500 Kbar. The average hardness after shock treatment was 51.7 Rc. Shock treatment was followed by carbide aging at 1600°F for 8 hours followed by final aging at 1400°F for 16 hours. The average hardness after carbide aging was 49.3 Rc and increased to 50.5 Rc after the final age. Tensile samples were cut and prepared from this series of shock TMP'd AF2-1DA plates. The tensile properties for the ST+ $\gamma'$ +S+C+F conditions are presented in Table 6.

The results were generally disappointing. The room temperature strength was very high but the tensile sample fractured while the load was still rising and consequently the elongation and RA were poor. The 1400°F properties were substantially better; however, the elongation and RA were still not sufficient. One encouraging aspect about the ductility was that some necking did occur indicating relatively good toughness. The excellent toughness of this processing schedule will be further exhibited by the stress rupture and low cycle fatigue results.

The choice of a  $\gamma'$  coarsening heat treatment prior to shock treatment is a definite requirement according to the results of experiments completed to this point. It is also obvious the  $\gamma'$  coarsening temperature should be less than 1950°F. Exactly what the  $\gamma'$  coarsening temperature-time sequence prior to shock wave treatment should be is not yet clear. The 1900°F/2hr. sequence is a step in the right direction but is not necessarily considered by the author to be optimum. For example Orava in the previous study<sup>2</sup> used a 1550°F pre-shock  $\gamma'$  aging treatment as well as what was believed to be a 1900°F  $\gamma'$  aging treatment for U-700. The suspected 1900°F aging temperature was the result of a furnace controller malfunction and the exact temperature could not be determined. It is possible that a lower pre-shock  $\gamma'$  aging temperature would result in a higher elongation and R.A. In addition it is also possible that changes in the carbide heat treatment will be needed to further optimize ductility and toughness parameters.

#### 4.3 STRESS RUPTURE BEHAVIOR

Stress rupture tests at 1400°F and 85,000 psi stress were conducted on AF2-1DA alloy in the STA, ST+ $\gamma'$ +S+F, ST+ $\gamma'$ +S+C+F and ST+S+C+F conditions. Rupture life, elongation as a function of time and elongation to failure were recorded for each of these conditions. The time to failure and total

elongation results are listed in Table 8.

The first stress rupture test failed by the specimen breaking at the hole for the pin grip. The second sample failed in the gage section after only 3.2 hours. Both of these specimen were from the  $ST+\gamma'$ (1900°F)+S+F condition. Additional specimens were tested at random for the various process conditions available. The results were erratic, however, one of the specimens,  $ST+\gamma'$ (1900°F)+S+C+F, achieved a 138.8 hour rupture life. This was superior to the 130.9 hours indicated by Cyclops as typical.

It was at first feared that shock wave processing had introduced subsurface microcracks into the AF2-1DA plates by the tensile rarefaction or reflection component of the shock wave. A section of material from one of the unshocked stress rupture samples and the shocked stress rupture sample that broke after 138.8 hours was examined metallographically. Microphotographs for the 2 samples are presented in Figures 9 and 10. The reason for the low experimental stress rupture values in the STA condition was readily apparent.

The unshocked (STA) stress rupture specimen (Figure 9) was observed to contain many carbides which in some cases are preferentially oriented as stringers parallel to the plate rolling direction. These stringers appear to be fragments of carbides strung out during rolling. Ruptures are initiated at the specimen exterior surface as well as at the interior carbide stringers, which are apparently acting as free surfaces. Ruptures propagate along grain boundaries and around the large MC carbides generally perpendicular to the tensile axis. Therefore not only are the external surfaces acting to initiate ruptures at grain boundaries and MC carbides, but internal defects in the form of carbide stringers are performing in the same manner. Such a mechanism greatly increases the number of stress risers in a given section and would obviously shorten the failure time as the ruptures grow and eventually link. This would explain the unusually short failure times for all of the STA samples and the erratic results for the shock TMP samples.

The interesting aspect to these results is the fact that the specimen having a rupture life exceeding the STA condition also suffered from the same material defect. Ruptures can be seen propagating from the carbide stringers as well as from the external surface in the  $ST+\gamma'+S+C+F$  stress rupture specimen shown in Figure 10. However, the much longer rupture life would indicate the crack propagation rate has been much slower. A lower crack propagation rate would indicate a higher fracture toughness which in turn would correlate with the increase in strength and ductility determined in tensile tests.

The best rupture life was realized by the  $ST+S+C+F$  condition which failed after 191.3 hours. This represents a 46% increase over the typical value given by Cyclops for the STA condition and an increase of nearly 9 times over the STA rupture life determined during this program. Undoubtedly the superior rupture life is the result of the excellent strength and ductility of the  $ST+S+C+F$  condition. A creep rate vs. time curve for the STA,  $ST+\gamma'+S+C+F$  and  $ST+S+C+F$  conditions are presented in Figure 11 for

Table 8. Stress Rupture Behavior for Thermally Processed and Shock Wave Thermomechanically Processed AF2-1DA.

Specimen Condition	Failure Time (Hours)	Total Elongation, %	Remarks
ST+ $\gamma'$ +F(STA)	130.9	6.8	Cyclops Typical
"	21.9	1.7	
"	32.1	2.5	
"	10.6	1.2	
"	(21.5)	(1.8)	DRI Average
ST+ $\gamma'$ (1900°F)+S+F	21.4	1.6	
"	3.2	.9	
"	21.4	1.6	
"	(15.3)	(1.4)	Average
ST+ $\gamma'$ (1900°F)+S+C(1600°F)+F	65.7	2.7	
"	138.8	5.5	
ST+S+C(1600°F)+F	191.3	5.0	
"	74.0	1.8	

ST - Solution Treated-2180°F/2hr-RAC

$\gamma'$ (Temp.) - Gamma Prime Age-2h-RAC

C(Temp.) - Carbide Age- 8hr-AC

F - Final Age - 1400°F/2hr-AC

S - Shock Wave Treatment-500Kbar



500X

Figure 9. STA Processed AF2-1DA Alloy Microstructure from Stress-Rupture Sample Revealing Grain Boundary Ruptures Originating at Carbide Stringers.



100X

Figure 10. ST+ $\gamma'$ +S+C+F Processed AF2-1DA Alloy Microstructure from Stress Rupture Sample Revealing Grain Boundary Ruptures Originating at Carbide Stringers and the Specimen Surface.

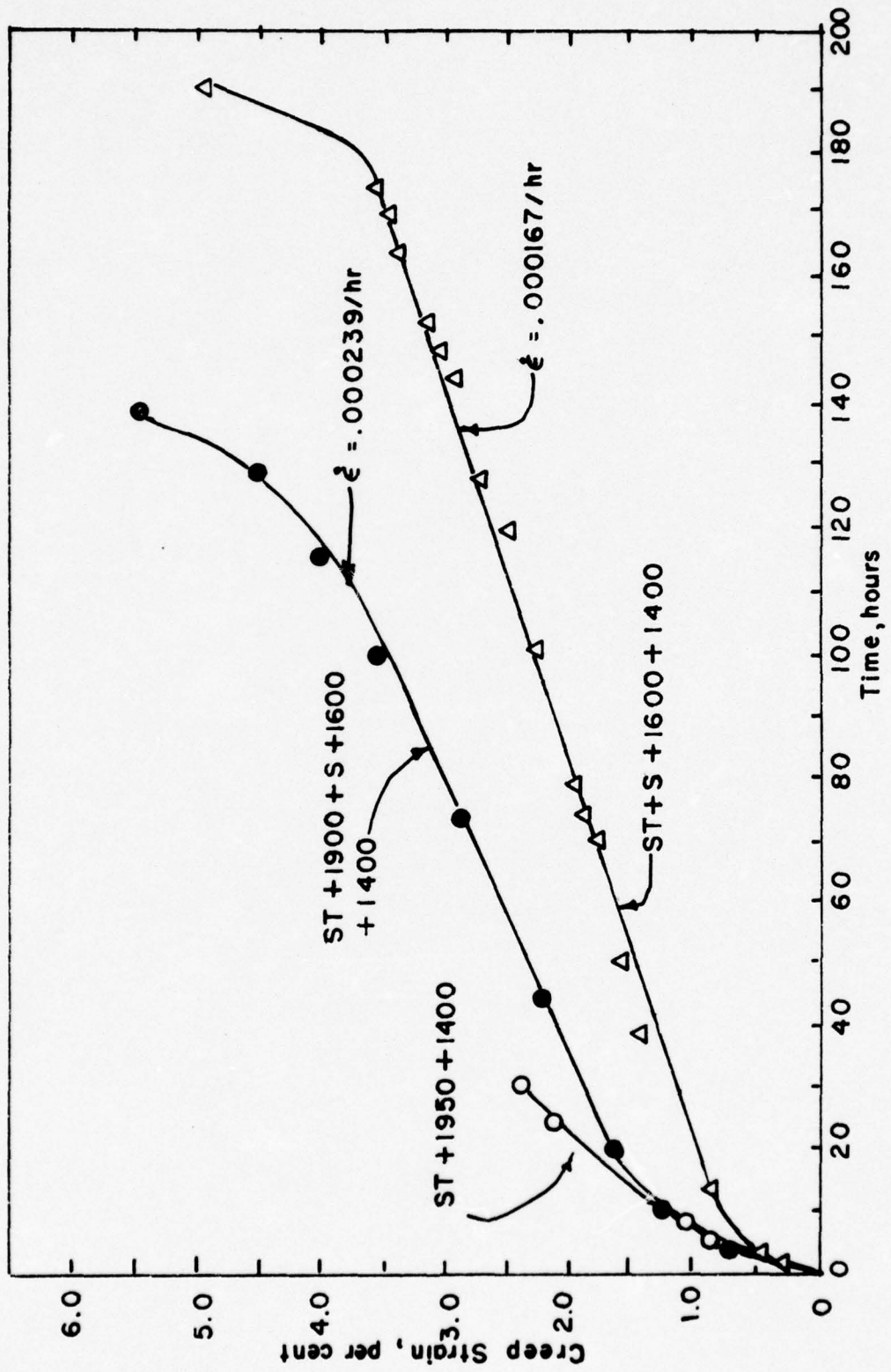


Figure 11. Creep Test Results at 1400°F and 85,000 psi for AF2-1DA Alloy after Various Processing Treatments

the best stress rupture life in each of those 3 categories. Minimum creep rates are given on the curves.

The discovery of internal defects in the AF2-1DA in the form of carbide stringers may explain some of the erratic results experienced throughout the program. Re-examination of the tensile samples processed early in the program indicate that carbide stringers were less prevalent but did exist. To what degree the tensile results were affected is unknown; however, it is suspected that low elongation tensile failures could be due to the carbide stringers or simple crack initiation due to very large carbides.

It is apparent from these results that shock wave TMP has been effective in improving the stress rupture properties of AF2-1DA. This would be true whether the comparison is made against the typical STA condition or the STA condition of this program. In addition the stress rupture results are consistent with the tensile results.

#### 4.4 LOW CYCLE FATIGUE BEHAVIOR

Just as increases in strength, elongation and R.A. (strain energy to fracture) signify improvements in toughness; a toughness increase indicates improvement in stress rupture and low cycle fatigue behavior. Results in the previous section demonstrated that increases in stress rupture behavior did in fact parallel tensile property increases. Low cycle fatigue tests were conducted on STA, ST+S+C+F and ST+ $\gamma'$ +S+C+F specimens cut from the same plates and processed at the same time as the stress rupture specimens. The mean stress was 60,000 psi and the alternating stress was 40,000 psi. The A ratio for these conditions is 0.67. The stress concentration factor was  $K_t = 3.0$ . Tests were conducted at 1400°F in air. Temperature was controlled to  $\pm 10^\circ\text{F}$  by a thermocouple positioned approximately 1/4 inch from the specimen notch. The results are presented in Table 9.

Having discovered that carbide stringers and possibly large MC carbides in the AF2-1DA plate had adversely affected the stress rupture tests, it was not surprising to observe erratic behavior in the LCF data. The large variation in cycles to failure at a particular condition as well as between the STA condition and the shock TMP conditions is thought to be affected by the existence of carbide stringers and large MC carbides. However, the low cycle fatigue results do parallel the rupture life as well as reflect the lower tensile properties of the STA condition. Although the number of cycles to failure may be adversely affected by the MC carbide distribution and therefore difficult to compare to other AF2-1DA results, it is believed the differences between the shock TMP and the STA conditions are real and do reflect the positive enhancement of shock TMP on AF2-1DA.

#### 4.5 SHOCK WAVE PROCESSING OF A DISK CONFIGURATION

Shock wave TMP has been shown to be an effective means of increasing the mechanical properties of AF2-1DA alloy in this program as well as U-700 and Inconel 718 during the previous programs<sup>2</sup>. A major question

Table 9. Influence of Shock Wave TMP on the Low Cycle Fatigue Life of AF2-1DA

Specimen Condition	Test Temperature °F	Cyclic Stress(Ksi)	Cycles to Failure
STA-1	1400°F	60 ± 40	762
"	"	"	381
ST+γ'+S+C+F	1400°F	60 ± 40	3943
"	"	"	1708
ST+S+C+F	1400°F	60 ± 40	4301
"	"	"	4997

ST - Solution Treated 2180°F/2hr-RAC

γ' - Gamma Prime Aged 1900°F/2hr-RAC

C - Carbide Aged 1600°F/8hr-AC

F - Final Age 1400°F/16hr-AC

S - 500 Kbar Shock

A ratio = 0.67

K<sub>T</sub> 3.0

to be answered is the applicability of the shock wave process to nickel base superalloy components. One of the key superalloy components that might benefit from shock wave TMP is the gas turbine disk. Present fabrication approaches involve isothermal forging or hot isostatic pressing (HIP) to a near net shape configuration. Both processes must be accomplished hot and HIP processing occurs at a temperature above the warm working temperature leaving no residual work hardening. The closer to net shape the forming process achieves, the less stock available in a subsequent conventional deformation process, which must produce a shape change to introduce an effective strain.

Shock wave deformation on the other hand can introduce an effective "plastic" strain with only a small residual shape change. For example, an effective "plastic" shock strain of 20% may be accompanied by a permanent dimensional change of 1% if properly done. Therefore, the capability of introducing work into a nickel base superalloy component of near net shape as part of a total TMP sequence would constitute a major advantage of the shock wave technique. To demonstrate that potential a simulated turbine disk was shock wave deformed.

Since the demonstration of capability was concerned primarily with component shape, the simulated turbine disk was machined from a cold finished steel round. A superalloy disk was not available for this demonstration and measurement of material response was not an objective. Cold finished steel was chosen because the ductility is lower than hot finished steel.

A slice from a 6 inch diameter cold finished round was machined to the "disk" cross section shown in Figure 12. The "disk" was fitted into a spall ring and the center hole plugged. The disk was backed by a spall plate, and all voids filled with a low melting metal (Cerro Low). A photograph of the assembly is shown in Figure 13. The shock wave pressure was chosen to be 150Kbar because a simple explosive-flyer plate configuration is possible at that pressure. In addition, a lower shock wave pressure will reduce the tendency for unwanted deformation (dishing) and cracking (spall). It is anticipated, but not yet demonstrated with nickel base superalloys, that several low pressure shock wave treatments will have the same cumulative effect as one high pressure shock wave treatment. A drawing of the disk assembly and the explosive driven flyer plate is shown in Figure 14. The flyer plate was 1/8 inch copper. The center initiation causes an oblique flyer plate impact; however, the resulting pressure will be the same as that produced by a planar impact at the same velocity. The time distribution of pressure will be different.

After shocking, the disk was recovered intact with no sign of deformation or fracture. Closer examination revealed the 6 inch disk diameter had increased by approximately 0.050 inches. The inner hole diameter was reduced by approximately 0.030 inches. The disk was separated from the spall ring, spall plate and center plug when recovered. The surface of the disk was wetted with the low melting alloy and was therefore cleaned by grit blasting. The resulting shocked disk is shown in Figure 15.

It should also be feasible to shock a 6 inch diameter disk to 400Kbar

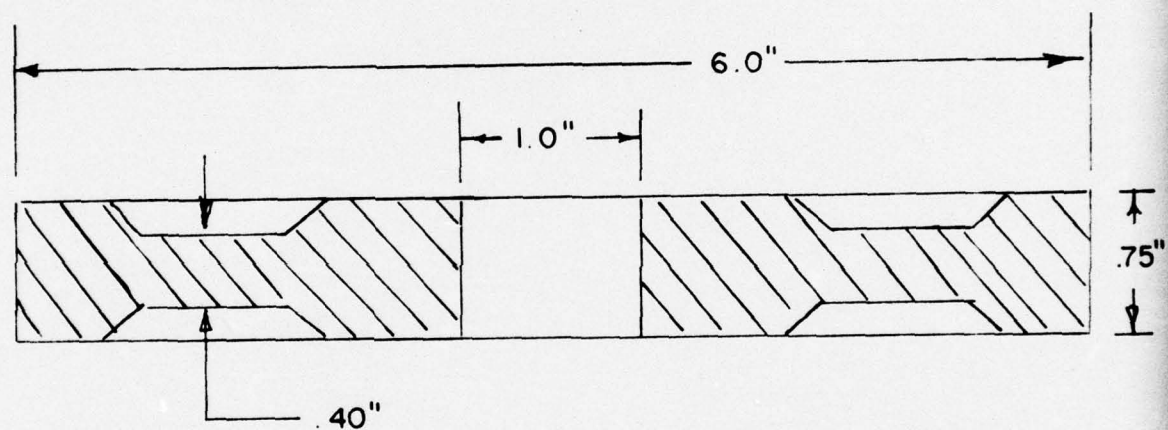


Figure 12. Simulated Superalloy Disk Cross Section for Shock Wave TMP.

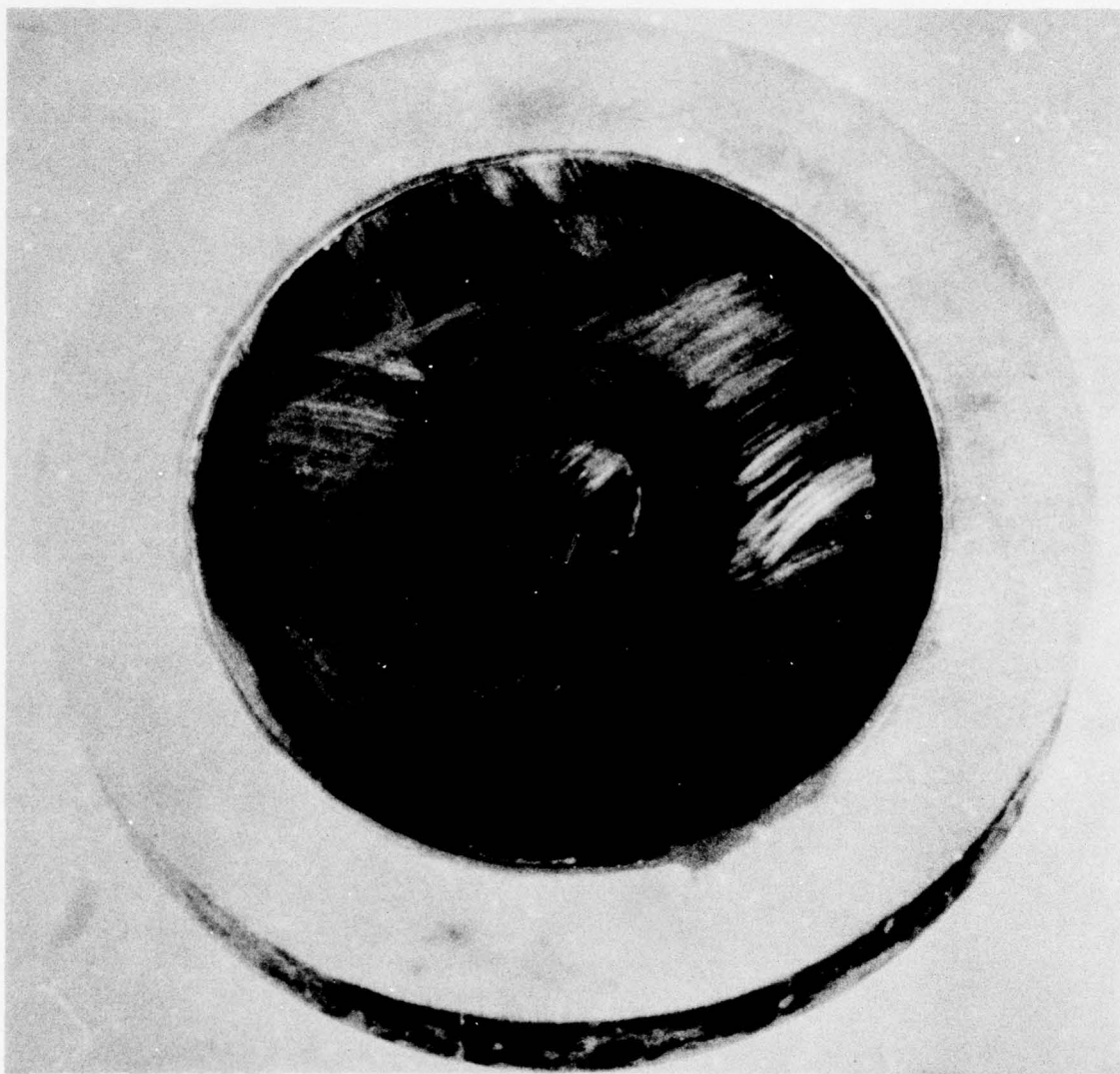


Figure 13. Photograph of Simulated Superalloy Disk Assembly Before Shock Wave Treatment.

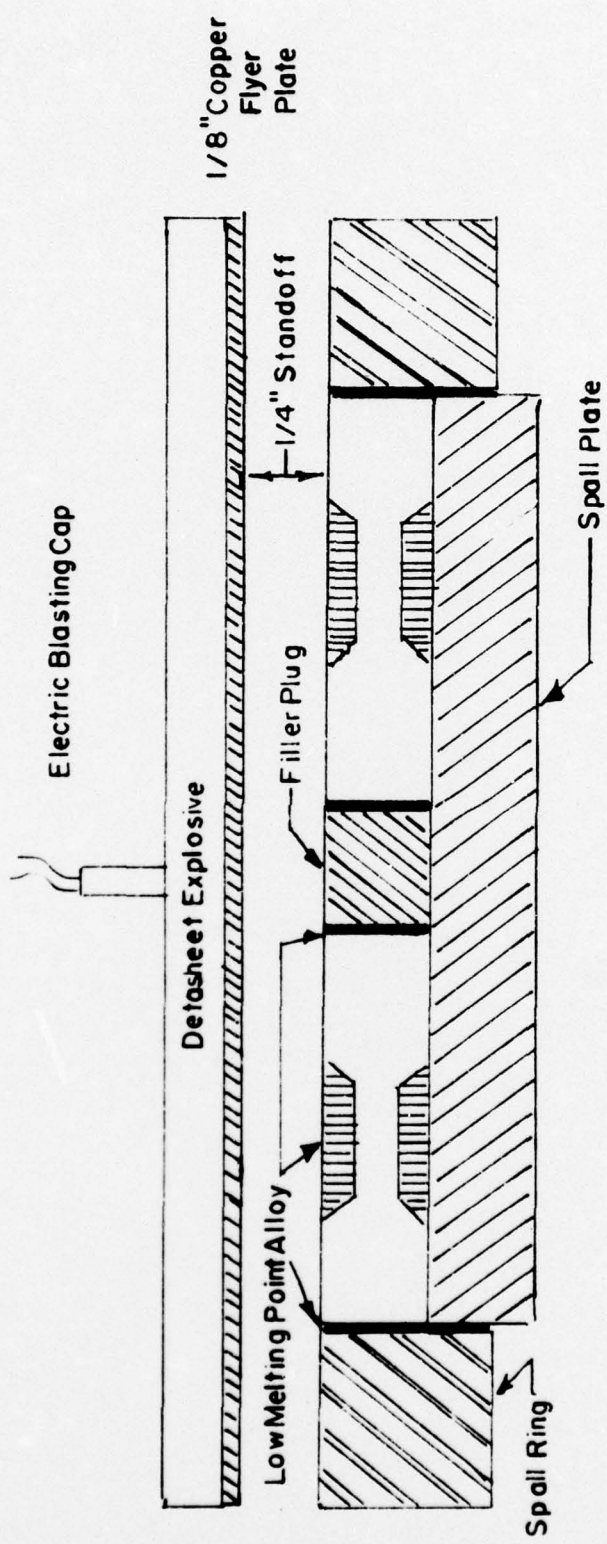


Figure 14. Simulated Superalloy Disk, Support Tooling and Explosively Driven Flyer Plate Configuration for 150 kbar Shock Wave Treatment.

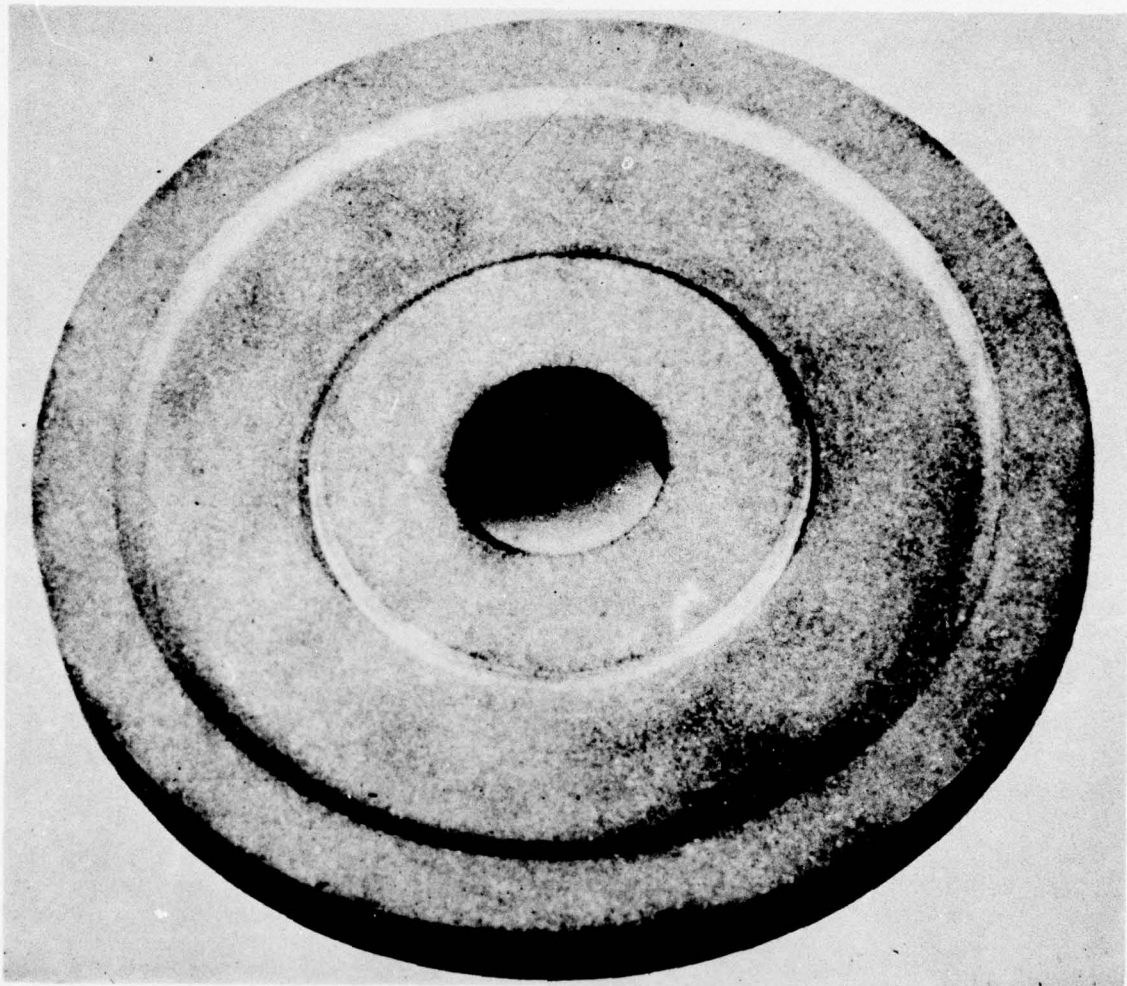


Figure 15. Simulated Superalloy Disk after 150 Kbar Shock Wave Treatment and Grit Blasting.

or a larger disk (12 inch to 36 inch) to multiple low pressure shocks. Selective area shocking (i.e. rim or hub) should also be feasible on a large disk.

## SECTION V

SUMMARY AND CONCLUSIONS

The results of this research program indicate that both material property enhancements and processing advantages can result from shock wave thermomechanical processing of AF2-1DA alloy. During the course of this study AF2-1DA alloy plates in various metallurgical conditions were subjected to 500 Kbar shock wave pressure treatments. Samples were additionally heat treated after shocking but prior to extensive mechanical property evaluation. Results of the mechanical property measurements on both shock wave processed and conventionally heat treated AF2-1DA alloy plates demonstrate the effectiveness of the shock wave process. A listing of the mechanical property changes resulting from shock wave treatment as compared to the solution treated and aged condition follows.

1. The tensile strength at room temperature was increased by 6% using the solution treat plus gamma prime plus shock plus final age sequence.
2. The yield strength at room temperature was increased 46% by the same shock wave treatment; however, the elongation decreased by 65%.
3. The tensile strength at 1400°F was increased by 3% using the processing sequence of paragraph 1.
4. The yield strength at 1400°F was increased by 15% using the above processing sequence while the elongation and reduction of area were increased by 7% and 20% respectively. Such a result would signify a substantial increase in the toughness of the AF2-1DA alloy at the 1400°F temperature.
5. The introduction of a carbide aging sequence after shock wave treatment but prior to final aging further increases the room temperature and 1400°F yield and ultimate strength levels but at the expense of ductility. However, metallographic examination of broken tensile samples indicates the low ductility may be the result of excessive amounts of MC carbide in the original microstructure. The cause of ductility loss (shock wave process, excessive MC carbide, or both) was not resolved.
6. The stress rupture life times of shock wave processed AF2-1DA were 5 to 6 times that of AF2-1DA stock in the STA condition. The shock processed material was only equal to or 1.2 times better than the normal values of rupture life reported for AF2-1DA alloy at 1400°F. This large difference exists because the STA processed material had a lower than normal rupture lifetime. It was discovered that large MC carbide stringers were responsible for the early failures of the STA condition investigated in this program and that those same stringers were present in the shock wave processed material. A possible conclusion from this result is that shock TMP has increased the toughness of the AF2-1DA, thus reducing the effectiveness of internal flaws introduced by the massive carbides. It is therefore

probable the large increase in rupture lifetimes are real.

7. The low cycle fatigue life at 1400°F of shock wave processed AF2-1DA was from 2 to 10 times greater than STA processed alloy used in this program. This result is consistent with a material toughness increase thought to be responsible for the stress rupture property improvements.

8. Prior metallurgical structure has a strong influence on the effectiveness of the shock wave deformation. It appears the optimum condition for shock wave introduction is one where the microstructure contains a gamma prime size that is somewhat smaller than that achieved by the standard gamma prime aging sequence of 1950°F for 3 hours. Shock wave produced dislocations apparently interact with the precipitated gamma prime phase to create an arrangement that is relatively stable at 1400°F testing temperature. The best gamma prime precipitation treatment for shock wave interaction achieved in this program resulted from a 1900°F - 3 hour heat treating sequence. The size and distribution of gamma prima produced at this condition was not characterized. The shock wave strengthening mechanism in AF2-1DA appears to be similar to that of U-700 alloy which is also gamma prime strengthened.

9. Successful shock wave treatment of a simulated alloy disk was accomplished indicating the process can be applied to a moderately complex shape. Introduction and transmission of the shock wave is best accomplished by "potting" the shape to be treated in a medium that is relatively incompressible. In this study a low melting alloy was used to fill voids in the simulated disk.

10. Shock wave deformation equivalent to a shape distortion strain of nearly 20% was successfully introduced into a material with less than 10% tensile ductility without fracture or a final dimensional change. Such a capability when viewed in conjunction with 9 indicates the potential use of the process for near net shape hardware.

REFERENCES

1. R. N. Orava, "Thermomechanical Processing of Nickel-Base Superalloys by Shock Wave Deformation," DRI Report 2618 to Naval Air Systems Command, Contract No. N00019-72-C-0138, March 1973.
2. R. N. Orava, "Response of Nickel-Base Superalloys to Thermomechanical Processing by Shock-Wave Deformation," DRI Report 2638 to Naval Air Systems Command, Contract No. N62269-73-C-0376, April 1974.
3. G. R. Fowles, "Shock Wave Physics", in Metallurgical Effects at High Strain Rates, ed. by R. W. Rohde, et al., Plenum Press, 1973.
4. C. S. Smith, Trans. Met. Soc. AIME, 1958, Vol. 212, P. 574.
5. John Grozinger, Supt. of Shops, B & O Railroad, Martensburg, W. Va., private communication.
6. Fred Sawyer, E. I. du Pont Explosives Products Division, private communication.
7. A. A. Deribas, Institute for Hydrodynamics, Novosibirsk, USSR, private communication.
8. R. J. De Angelis and J. B. Cohen, Trans. ASM, 1965, Vol. 58, p. 700.
9. R. H. Wittman, Denver Research Institute, University of Denver, Ltr. Report to AFML, May 1972.
10. S. Mahajan, "Metallurgical Effects of Planar Shock Waves in Metals", phy. stat. sol. V2, 1970, p. 187.
11. R. L. Nolder and G. Thomas, "The Substructure of Plastically Deformed Nickel", Acta Met., Vol. 12, 1970, p. 227.
12. R. J. McElroy and Z. C. Szkopiak, "Dislocation-Substructure-Strengthening and Mechanical-Thermal Treatment of Metals", Int. Met. Reviews, Vol. 17, 1972, p. 175.
13. J. Weertman, "High Velocity Dislocations", Response of Metals to High Velocity Deformation, ed. by P. G. Shewman and V. F. Zackay, Interscience, p. 205.
14. H. Kressel and N. Brown, "Lattice Defects in Shock Deformed and Cold Worked Nickel", J. Appl. Phys., Vol. 38, 1967, p. 1618.
15. B. A. Stein and P. C. Johnson, "Shock Hardening and Explosive Ausforming of Alloy Steels", Trans. AIME, Vol. 227, 1963, p. 1188.
16. S. M. Silverman, L. Godfrey, H. A. Hauser, and E. T. Seward, "Effect of Shock Induced High Dynamic Pressure on Iron Base Alloys", P & W Aircraft, E. Hartford, CT., Report No. ASD-TDR-62-442, ASD, W-P AFB, Ohio, Aug. 1962, AD No. 287 473.

17. B. G. Koepke, R. P. Jewett, and W. T. Chandler, "Strengthening of Iron Base Alloys by Shock Waves", Rocketdyne Report No. ML TDR 64-282, AFML, WPAFB, Ohio, Oct., 1964.
18. A. E. Doherty, J. Mykkanen, and E. K. Henriksen, "Dynamic Pressure Hardening of Irregular Shapes", Aerojet-General Corp. Report No. TR-66-127, AFML, WPAFB, Ohio, July, 1966, AD No. 489 402.
19. J. P. Mykkanen, A. E. Doherty and E. K. Henriksen, "A New Method for Strengthening of Metals with Application to Production-Type Parts", Proc. 2nd. Int. Conf. of the Center for High Energy Forming, ed. by A. A. Ezra, U. of Denver, 1969.
20. R. H. Wittman, "The Effect of Heat Treatment on the Mechanical Properties and Microstructure of Explosion Welded 6061 Aluminum Alloy", source cited in Ref. 1, P. 669.
21. J. D. Buzzanell and H. L. Black, "Manufacturing Methods for Rolling Very High Strength Superalloy Sheet", Universal-Cyclops Corp., Report No. AFML-TR-72-80, WPAFB, Ohio, July, 1972.
22. H. E. Collins and R. J. Quigg, "Carbide and Intermetallic Instability in Advanced Nickel-Base Superalloys", Trans ASM, Vol 61, 1968, P. 139.
23. R. L. Dreshfield, "The Effect of Refractory Elements on the Stability of Complex Carbides in Ni-Base Superalloys", ibid, p. 352.
24. R. N. Orava and R. H. Wittman, "Techniques for the Control and Application of Shock Waves", Proc. 5th Int. Conf. of the Center for HERF, University of Denver, 1975.
25. A. R. Champion and R. W. Rohde, "Hugoniot Equation of State and the Effect of Shock Stress Amplitude and Duration on the Hardness of Hadfield Steel", J. Appl. Phys., Vol. 41, 1970, p. 2213.
26. G. E. Duvall, "Some Properties and Applications of Shock Waves", source cited in ref. 11., p. 165.
27. R. W. Gurney, "The Initial Velocity of Fragments from Bombs, Shells and Grenades", Ballistic Research Laboratories, Aberdeen Proving Ground, MD, Report No. 405, Sept. 14, 1943.
28. G. E. Duvall and J. O. Erkman, "Acceleration of a Plate by High Explosive", Stanford Research Institute, Technical Report No. 1, Contract No. DA-04-200-501-ORD-731, Picatinny Arsenal, May, 1958.
29. A. K. Aziz, H. Hurwitz, and H. M. Sternberg, "Energy Transfer to a Rigid Piston Under Detonation Loading", J. Phys. Fluids, Vol. 4, 1961, p. 380.
30. J. E. Kennedy, "Explosive Output for Driving Metal", Proc. Symp. on Behavior and Utilization of Explosives in Engineering Design, ed. by L. Davison et al., New Mexico Section, ASME, Albuquerque, NM, 1972.

31. R. E. Peterson, Stress Concentration Design Factors, John Wiley & Sons, NY, 1953.

DISTRIBUTION LIST

Contract No. N62269-74-C-0281

(One copy unless otherwise noted)

(3 copies plus balance after distribution)

U. S. Naval Air Systems Command  
(AIR-52031B)

Department of the Navy  
Washington, D. C. 20361

(7 copies, for internal distribution by AIR-954  
AIR-954 (2 copies), AIR-536B1 (1 copy), AIR-330B  
(1 copy), AIR-5361A (1 copy), AIR-5362A (1 copy),  
AIR-330A (1 copy)

U. S. Naval Air Systems Command  
AIR-954

Department of the Navy  
Washington, D. C. 20361

Commander  
Naval Air Development Center  
(Code 302A)  
Warminster, Pennsylvania 18974

U. S. Naval Air Turbine Test Station  
ATTN: E. Lister (AT-1P)  
1440 Parkway Avenue  
Trenton, New Jersey 08628

U. S. Naval Sea Systems Command  
Code 035  
Department of the Navy  
Washington, D. C. 20362

(2 copies)  
Commander  
Naval Weapons Center  
Code 4585 (1 copy) Code 5567 (1 copy)  
China Lake, California 93555

Naval Ships Engineering Center  
Code 6146  
Center Bldg. Room 202  
Prince Georges Center  
Hyattsville, Maryland 20782

U. S. Naval Ships Research and Development Center  
Code 2812  
Annapolis, Maryland 21402

Commander  
Naval Ordnance Laboratory  
(Metallurgy Division)  
White Oak  
Silver Spring, Maryland 20910

Director  
Naval Research Laboratory  
Code 6300 (1 copy)  
Washington, D. C. 20390

Office of Naval Research  
The Metallurgy Program, Code 471  
Arlington, Virginia 22217

(2 copies)  
Army Materials and Mechanics Research Center  
Dr. A. Gorum (1 copy) Dr. E. S. Wright (AMXMR-E) (1 copy)  
Watertown, Massachusetts 02172

Army Materiel Command  
Building T-7 Gravelly Point  
Attn: AMCRD-TC  
Washington, D. C. 20315

U. S. Army Aviation Materiel Laboratories  
Fort Eustis, Virginia 23604

Air Force Materials Laboratory  
(Code LL - H. M. Burte)  
Wright-Patterson Air Force Base  
Dayton, Ohio 45433

Air Force Propulsion Laboratory  
Code TB  
Wright-Patterson Air Force Base  
Dayton, Ohio 45433

Aeronautical Systems Division  
Code ENJ  
Wright-Patterson Air Force Base  
Dayton, Ohio 45433

National Aeronautics and Space Administration  
Code RWM  
Washington, D. C. 20545

National Aeronautics and Space Administration  
Lewis Research Center  
G. M. Ault  
21000 Brookpark Road  
Cleveland, Ohio 44135

U. S. Atomic Energy Commission  
Division of Reactor Development  
(A. Van Echo)  
Washington, D. C. 20545

Metals and Ceramics Information Center  
Battelle Memorial Institute  
505 King Avenue  
Columbus, Ohio 43201

The Johns Hopkins University  
Applied Physics Laboratory  
(Maynard L. Hill)  
8621 Georgia Avenue  
Silver Spring, Maryland 20910

AVCO RAD  
201 Lowell Street  
Wilmington, Massachusetts 01887

ITT Research Institute  
10 West 35th Street  
Chicago, Illinois 60616

Detroit Diesel Allison Division  
General Motors Corporation  
Materials Laboratories  
Indianapolis, Indiana 46206

Pratt and Whitney Aircraft Division  
United Aircraft Corporation  
East Hartford, Connecticut 06108

Pratt and Whitney Aircraft  
Materials Branch  
Florida Research and Development Center  
West Palm Beach, Florida 33402

United Aircraft Research Labs  
United Aircraft Co.  
East Hartford, Connecticut 06108

Airesearch Division  
Garrett Corporation  
Phoenix, Arizona 85001

Lycoming Division  
AVCO Corporation  
Stratford, Connecticut 06497

Curtis Wright Company  
Wright Aeronautical Division  
Wood-Ridge, New Jersey 07075

Bell Aerosystems Company  
Technical Library  
P. O. Box 1  
Buffalo, New York 14240

General Electric Company  
Aircraft Engine Group  
Materials and Processes Technology Laboratories  
Evendale, Ohio 45215

Solar  
(Dr. A. Metcalfe)  
2200 Pacific Highway  
San Diego, California 92112

Teledyne CAE  
1330 Laskey Road  
Toledo, Ohio 43601

Stellite Division  
Cabot Company  
Technical Library  
P. O. Box 746  
Kokomo, Indiana 46901

Crucible Inc.  
Materials Group (Mr. E. J. Dulis)  
P. O. Box 88  
Pittsburgh, Pa. 15230

Colt Industries  
Materials Research Center Library  
Box 88  
Pittsburgh, Pa. 15230

Dr. Nicholas Grant  
Massachusetts Institute of Technology  
Center for Materials Science and Engineering  
Cambridge, Massachusetts 02139

Whittaker Company  
Nuclear Metals Division  
P. O. Box 125  
West Concord, Massachusetts 01781

Special Metals Company  
(Mr. Charles Speer)  
New Hartford, New York 13413

Benet R & E Laboratories  
(Dr. J. E. Pepe)  
Department of the Army  
Watervliet Arsenal  
Watervliet, New York 12189

Aluminum Company of America  
(Mr. Greg Barthold)  
1200 Ring Building  
Washington, D. C. 20036

TRW Equipment Laboratories  
23555 Euclid Avenue  
Cleveland, Ohio 44117

Universal-Cyclops Specialty Steel Division  
650 Washington Road  
Pittsburgh, PA 15228  
Attn: Mr. J. D. Buzzanell

Climax Molybdenum Co. of Michigan (Inc.)  
Division of AMAX  
1600 Huron Parkway  
Ann Arbor, Michigan 48106  
Attn: Dr. W. Fergus Porter  
Director of Research

Final Report Only (12 copies)  
Commander  
Naval Air Development Center  
Code 302A, A Fletcher for DDC  
Warminster, PA 18974

Final Report Only (3 copies)  
Commander  
Naval Air Development Center  
Code 813  
Warminster, PA 18974